Investigation of the Impact of Turbine Blade Geometry on Near-Field Microwave Blade Tip Time of Arrival Measurements

A Thesis
Presented to
The Academic Faculty

by

Aline Katharina Zimmer

In Partial Fulfillment
of the Requirements for the Degree
Master of Science in Aerospace Engineering

Daniel Guggenheim School of Aerospace Engineering
Georgia Institute of Technology
December 2008

Investigation of the Impact of Turbine Blade Geometry on Near-Field Microwave Blade Tip Time of Arrival Measurements

Approved by:

Dr. Jechiel Jagoda, Advisor
Daniel Guggenheim School of Aerospace Engineering
Georgia Institute of Technology

Dr. Laurence Jacobs, Co-Advisor
School of Civil and Environmental Engineering
Georgia Institute of Technology

Dr. Jerry Seitzman
Daniel Guggenheim School of Aerospace Engineering
Georgia Institute of Technology

Date Approved: October 3, 2008

To my family and friends

in deepest recognition and highest appreciation of their invaluable support

Für meine Familie und meine Freunde

in tiefster Anerkennung und höchster Wertschätzung ihrer einzigartigen Unterstützung

ACKNOWLEDGEMENTS

This work is not my work alone. I owe a great debt of gratitude to those who have supported and guided me.

Firstly, I would like to acknowledge my advisors, Dr. Laurence Jacobs and Dr. Jechiel Jagoda, for their continuing encouragement and effort that make this work possible as well as Dr. Jerry Seitzman for taking the time to evaluate this study. The support and feedback from my advisory committee were priceless to me.

Furthermore, I would like to thank Dr. Jerrol Littles, Ben Hall, and Lauren Gray at Pratt & Whitney as well as Tom Holst and Michaël Hafner at Vibro-Meter SA for their support and for answering my countless questions.

I would like to acknowledge Pratt & Whitney for their financial support of this project and the German Academic Exchange Service (DAAD) for enabling me to attend the Georgia Institute of Technology.

Also, I would like to thank Martin "H. P." Treiber. He became a true friend during the time we spent at the Georgia Institute of Technology together.

Last but not least, I would like to express my loving gratefulness to the people who are dearest to me: I wish to express my gratitude towards Dolf Diederichsen for sincerely believing in me at all times as well as for his encouragement during the ups and downs of this research. Finally, I would like to thank my parents and family to whom I am deeply indebted. I truly appreciate their unique and invaluable support during my entire course of studies.
Der größte Dank gebührt jedoch meinen Eltern und meiner Familie. Ihnen bin ich für ihre einzigartige und unschätzbare Unterstützung während meines gesamten Studiums unendlich dankbar.

TABLE OF CONTENTS

LIST OF TABLES

LIST OF FIGURES

LIST OF SYMBOLS & ABBREVIATIONS

ADC	Analog to digital converter
DAC	Digital to analog converter
DFT	Discrete Fourier transformation
FFT	Fast Fourier transformation
IBR	Integrally bladed rotor
NSMS	Non-intrusive stress measurement system
PHM	Prognostic health management
RCS	Radar cross-section
STFT	Short-time Fourier transformation
ToA	Time of arrival
ToF	Time of flight

c_{air}	Speed of electromagnetic waves in air
D	Antenna aperture diameter
$d_{absolute}$	Absolute distance to target
$d_{far-field}$	Distance to beginning of antenna far-field
$d_{reactive\ near-field}$	Distance to end of antenna reactive near-field

G	Antenna gain
n	Integer number of full wavelengths traveled
P_r	Power received back at radar
P_t	Power transmitted
α	Blade chord angle
θ_0	Initial system phase lag
θ_{rel}	Relative phase change to target
λ	Wavelength
λ_{air}	Wavelength in air
σ	Radar cross-section of target

SUMMARY

A relatively new approach to measuring stress on a turbine blade or disk as part of Prognostic Health Measurement (PHM) involves the utilization of Non-Intrusive Stress Management Systems (NSMS). In NSMS, externally mounted probes measure the time of arrival (ToA) of the turbine blades, which can be converted to deflection and stress values. In order to be feasible for the utilization in field-ready PHM systems, the probes used for airfoil ToA measurements must be of high-durability and high spatial and temporal resolution. Since optical sensors are not sufficiently durable for the harsh environments of gas turbine engines, research focusing on non-optical sensors is currently advancing. However, these non-optical sensors exhibit low spatial resolution – further insight into the sensor-blade interaction of this large spatial diameter is needed.

This study investigates the manifestation of geometric features of turbine blades in signatures of non-optical ToA probes. The approach presented in this work enables an evaluation of the various signal characteristics used for defining arrival time for a range of airfoil geometries and provides knowledge about additional waveform characteristics that can provide further insight into airfoil and/or engine health.

The objective of this research is to increase the accuracy of microwave ToA probes by gaining a better understanding of the microwave signals. In order to fulfill this objective, five steps are taken. Firstly, ToA definitions used in the past are compared. Considering accuracy, computational effort, and versatility, the constant fracture crossing ToA definitions is found to provide the most accurate means for defining the ToA. Secondly, an experimental apparatus capable of measuring airfoil ToA with

stationary microwave probes and optical probes as a reference, as well incorporating a range of different turbine disks is designed and built. As a third step, a catalog of 16 turbine blade (tip-)geometries is developed. To gain a fundamental understanding of the microwave sensor response to a passing blade, the simplest geometries include blades with a rectangular cross-section of different widths. To approach more realistic turbine blade geometries, varying cross-sections, blade tip pockets, and chord angles are added. Fourthly, the signatures of these turbine blades are acquired using both the optical and the microwave probes and finally, the impact of the geometric effects on the signatures are investigated and evaluated.

The quality of the microwave results is found to be highly dependent on the polarization of the microwaves. Analysis of the time domain signal shows that decreasing the blade width, increasing the chord angle, or incorporating a blade tip pocket or a varying cross-section leads to a decrease in the amplitude of the peak caused by the blade. Increasing the blade width and incorporating a chord angle leads to an increase in peak width. The low blade-width-to-sensor-aperture ratio results in a high degree of spatial filtering. Therefore, other than in the amplitude and width of the peaks, the geometric features are not reflected in the signal with the exception of the widest blade with varying cross-section and blade tip pocket. The combination of these two features on the widest blade causes a change in the shape of the peak due to the higher blade-width-to-sensor-aperture ratio. A frequency domain analysis is conducted on the microwave signals and verified using a synthetic signal. This analysis supports and confirms the findings from the time domain analysis. The time domain analysis of the laser measurements shows that the spatial resolution of the laser is much higher than that of the microwave sensor. The rise and fall times of the signal are much shorter which is due to the much smaller field-of-view. Consequently, the signal acquired with the optical setup provides a good means of defining the blade ToA satisfactorily and meets the requirements to fulfill this objective.

The knowledge gained in this study about the sensor and its interaction with passing blade tips of varying geometry can be used to enhance the understanding of microwave ToA measurements. This knowledge provides further insight into airfoil and engine health. Hence, this study is a stepping-stone on the way to the eventual integration of microwave systems into field-ready PHM systems feasible for in-situ surveillance.

CHAPTER I

INTRODUCTION

1.1 Motivation and Problem Description

Recent studies have demonstrated the potential for utilizing blade time of arrival (ToA) sensors as part of real-time, integrated, physics-based Prognostic Health Management (PHM) systems for gas turbine engines – by measuring the blade ToA, information about the state of stress of the airfoil can be provided, which allows for life predictions [23].

For years, optical sensors have been used to assess airfoil stress conditions through blade ToA measurements during developmental testing of gas turbine engines. These optical probes provide a characteristically small active field (spot size), which enables the timing of a passing airfoil to be resolved with a high degree of accuracy. However, optical probes exhibit low durability. Especially in the "hot" section of turbines where temperatures can reach 1300 °C and speeds are commonly up to 30,000 rpm, the limiting factor in prognosis is sensor technology.

The current approach to obtain data from these harsh environments is through simulations that predict the current state based on measured test data. Real-time data could greatly improve this form of prognostics and control.

Higher-durability blade ToA probe types have been developed and demonstrated over the past several years, but these probes typically suffer from a larger active field for the blade stand-off distances pertinent to a gas turbine engine's PHM needs [13]. The larger active field results in a spatially lower ToA measurement resolution.

Consequently, sensor development is needed to meet the demands for high-precision data from harsh environments [3].

Another motivation is based on that fact that maintenance of parts in hot sections account for $40-60\,\%$ of the total engine maintenance cost although they contain a relatively small number of components compared to the whole system. Advanced monitoring techniques hold great potential for reducing cost [3].

1.2 Background Information

1.2.1 Prognostic Health Management

PHM is an important concept in machine evaluation and maintenance. It refers to the approach of evaluating and predicting the future condition and remaining lifetime of a component or system based on the current condition of system wear. It is based on the effective use of health monitoring, which can significantly enhance ongoing system engine maintenance by providing additional feedback. The conservative alternative is based on a maintenance schedule of exchanging the entire system or its components rather than on the actual condition.

The goals of PHM are improved reliability, safety, and maintenance efficiency with significant savings of money and time. In addition, effective PHM changes the mind-set from fear-of-failure to risk management [2]. However, advanced sensors must be developed to reliably detect flaws in a sufficiently early stage, in order to manage maintenance costs. Feasible sensors for this application include microwave sensors amongst other non-traditional detection technologies useful for engine monitoring applications [11].

1.2.2 Non-Intrusive Stress Measurement Systems

Gas turbine engines are key components of aircraft and their reliability is crucial in order to guarantee safety. Consequently, it is essential to be able to detect the onset of mechanical faults at a sufficiently early stage.

In turbine health monitoring, a primary metric is blade tip measurement for the purpose of vibration detection. A certain level of vibration is normal and turbine engines are designed to handle this environment. Nevertheless, these vibrations put components in a constant state of oscillating stress, which may eventually cause the components to fail.

In the past, measurement of stress on a turbine blade or disk was accomplished by placing strain gages on a component. The strain gage signals are transmitted to a data logging system through radio telemetry or slip rings. Although this approach is very accurate, the strain gages can change the dynamic properties of the rotor and the blades [15] and can degrade the the engine's performance. Since the gages and wires are located inside the engine, repairing often requires disassembling the engine, resulting in test delays and increased costs [14].

A relatively new approach involves the utilization of Non-Intrusive Stress Measurement Systems (NSMS). In NSMS, externally mounted sensors provide a "flexible, cost effective, reliable alternative to strain gages" [1]. These sensors can measure the ToA of the turbine blades and their radial clearance in order to deduce blade vibration [10]. In this context, it is important to note that a change in the vibration may indicate a change in the system caused by damage – computer models show that structural damage in turbine blades can lead to a change in the resonance characteristics of the blades [20]. By monitoring these vibrations, it is possible to detect degradations before they cause severe inefficiency or system failure.

Also, monitoring changes in blade clearance over time can detect turbine wear. Causes for tip clearance to change include loss of blade material due to mechanical interaction (rubbing on the case), due to material creep as a consequence of the constant stress of operation, or due to the presence of cracks in the blades and/or the disk. Wear caused by interaction between blade tips and casing as well as cracks can seriously impact mechanical behavior or even lead to premature failure [7].

Using a combination of clearance and vibration monitoring, serious cracks may be found and creep can be detected. The components may then be replaced before failure. Likewise, given the proper sensor technology to detect wear, these failure scenarios can be avoided.

The NSMS has proven to be a viable system for measuring blade vibrations [14]. Applications include: monitoring peak and rms vibrations of all blades in each row; detecting problems including resonating, bent, loose, cracked, and out-of-tune blades; detecting system modes of vibration while identifying interblade vibration phases, amplitudes, and nodal diameters; providing Campbell diagrams relating vibrational resonances to rotor speed; and providing archived digital data for all blades.

During its development stage, NSMS have successfully been applied to a variety of tests in a range of environments [14].

1.2.3 Arrival Times to Deflection to Stress Conversion

ToA data received from the sensor must be converted to blade deflections. This conversion involves the filtering of noise and correction for rotor acceleration effects. The filtering of noise is achieved by calculating windows of displacement within each revolution where the blade pulses are expected to occur. Pulse signals falling outside these windows are counted as noise whereas signals within the the windows are counted as blade-tip data. These displacement windows can be calculated based on 1/rev time obtained by a once per revolution probe, rotor diameter and blade separation around the rotor. An error in the construction of these displacement windows can occur if the rotor is accelerated within the respective revolution. A correction can be made by determining the change in speed between revolutions using the 1/rev measurements to correct each blade displacement window.

In the absence of any structural vibration, the ToA of a particular blade tip at one

probe depends only on the rotational speed and the radius of the rotor. However, if the blades are vibrating back and forth, their arrival occurs earlier or later than expected from the non-vibrating ideal.

The deflection of the individual blade is calculated from the difference between the measured blade tip ToA and the center of the window. The deflection data can be further processed to determine the vibratory and static components of the deflection. The so-called center-time is calculated by averaging the arrival times of all blades over a defined number of revolutions. The difference between the ideal ToA and the center time is a measure of the static component of the blade deflections.

Data from multiple probes at the same axial position on the blade (leading edge, mid-blade, trailing edge) are used in the digital signal processing unit of a NSMS to determine mode and frequency of the vibration. Once determined, the amplitude, phase, and other vibratory characteristics can be calculated. Further information on NSMS in general and the conversion can be found in numerous sources, such as [10, 14].

Knowing all necessary deflections, the corresponding stress levels can be calculated using an finite element (FE) model.

1.3 Research Objectives

This study investigates the manifestation of geometric features of turbine blades in signatures of non-optical ToA probes. The presented approach permits an evaluation of the various signal characteristics used for defining arrival time for a range of airfoil geometries and provide knowledge about additional waveform characteristics that can provide further insight into airfoil and/or engine health.

The objective of this research is to:

1. compare ToA definitions used in the past and determine the most accurate

means for defining ToA;

2. set up an experimental apparatus capable of measuring airfoil ToA with stationary non-optical ToA probes and optical probes as a reference;

3. develop a catalog of turbine blade (tip-)geometries of interest;

4. acquire signatures with both optical and non-optical probes; and

5. evaluate impact of geometric effects on the signal.

As a part of NSMS for PHM, the scope of this research is limited to the data acquisition and ToA definition, as this is the challenge specific to utilizing microwave sensors. This research does not investigate turbine blade vibrations, their state of stress or lifetime prediction.

CHAPTER II

LITERATURE REVIEW & TIME OF ARRIVAL DEFINITION

In the past and the present, researchers and companies used a variety of approaches to define the actual ToA of the tip of a blade under a stationary probe. This definition is not as straightforward as it seems at first. The underlying idea of a blade tip arriving at a certain position is quite imprecise and fuzzy due to the finite size of the blade and the sensor. However, it is essential to formulate the event as discretely and concisely as possible. This makes it possible to define at which relative position of the blade tip to the probe one can say that the blade has "arrived." As a next step, it is required to relate this relative position to a feature in the signature, which can be used to trigger the clock for each blade and each revolution. Each of these features is dependent on both the airfoil geometry and the sensor's active field. If the definition and thus, the timing is flawed, the prerequisite for a successful NSMS is not fulfilled. The intention of this chapter is to give an overview of the different definitions used by researchers and discuss their advantages and drawbacks.

2.1 Overview

First of all it is important to note that although every NSMS requires the definition of the ToA, not much is published about it. However, five approaches can be identified. Each of them uses a specific feature of the waveform of the sensor output as a trigger. These five features are: maximum amplitude rate; fixed voltage crossing (threshold); maximum amplitude; constant fraction crossing; and zero crossing.

Whereas the first two of the approaches define the ToA on the rising edge of the pulse, the third uses the maximum response as a trigger and the fourth defines the ToA on the falling edge. The last approach assumes a different waveform and cannot be classified in either of these categories.

Please note that some authors are not consistent in their ToA definitions and do not necessarily use the same feature as a trigger throughout all their published work.

2.2 Maximum Amplitude Rate

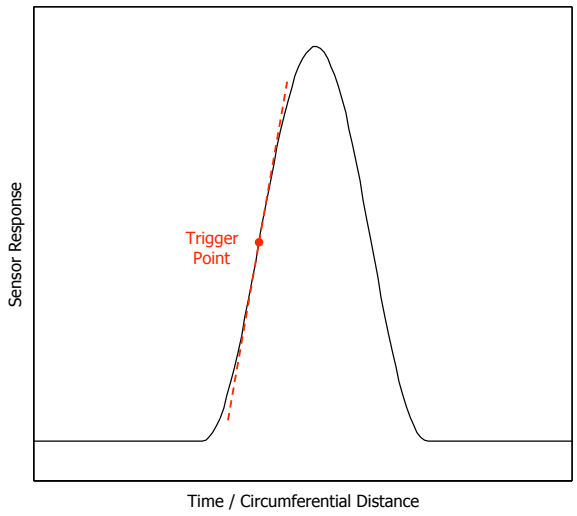

Figure 2.1: Maximum amplitude rate ToA definition

This ToA definition uses the positive slope of the signal as trigger. As the blade tip moves into the field-of-view of the sensor, the sensor response increases. At the maximum increase in the sensor response, the change in relative blade tip position is greatest. Therefore, this approach uses the waveform feature of the maximum amplitude rate to trigger the ToA clock as depicted in Figure 2.1. Figure 2.1 shows a simplified sensor response typical for an optical or a non-optical probe. The signal trace is plotted over the circumferential blade position. The waveform of a blade passing in front of the probe characteristically is represented by one peak, without

change of sign as oppose to the waveform referred to in Section 2.6.

This approach is used by Agilis Measurement Systems [1] in all of their NSMS, as well as Holmquist and Jalbert [12] and Littles et al. [17].

2.3 Fixed Voltage Crossing

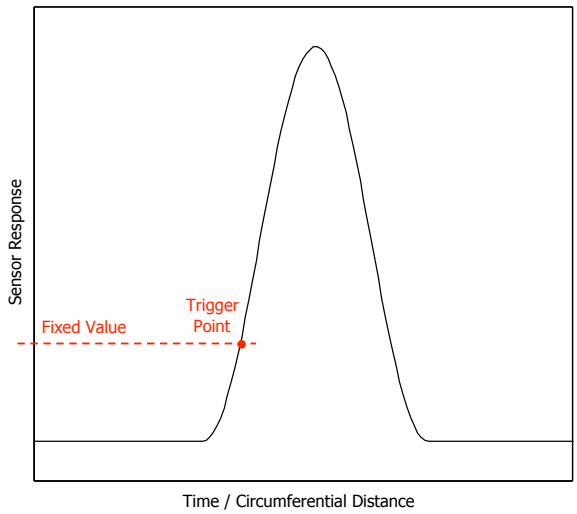

Figure 2.2: Fixed voltage crossing ToA definition

Von Flotow et al. [21] define the ToA based on a fixed voltage value on the rising edge of the blade-induced pulse, as seen in Figure 2.2. In the same manner, Holmquist and Jalbert [12] measure the ToA once the sensor response - most commonly measured as voltage - "ramps up past some threshold value." Dimitriadis et al. [5] and Joung et al. [15] also make use of this waveform feature.

This approach is more independent of the actual waveform than the first one, because it relies solely on an absolute value of voltage does not take the real blade-probe interaction into consideration.

2.4 Maximum Amplitude

Holquist and Jalbert also mention the definition of the blade tip ToA as a "measurement of total reflected energy which [...] peaks as a blade passes in front of the probe" [12]. The clock is triggered as the sensor response reaches its maximum, as seen in Figure 2.3. This is the only reference to maximum amplitude triggering found in the literature.

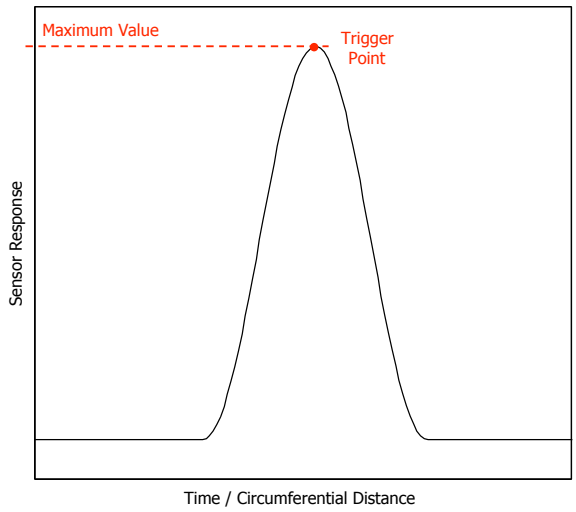

Figure 2.3: Maximum amplitude ToA definition

2.5 Constant Fraction Crossing

Another feature of the waveform which can be used for ToA definition is the constant fraction crossing.

This triggering according to the definition described by Zielinski and Ziller [23] "occurs on the falling edge, when the signal level drops below half the maximum value (constant fraction trigger)" as depicted in Figure 2.4. The percentage of the maximum response at which the clock is triggered is not necessarily chosen to be 50 % and

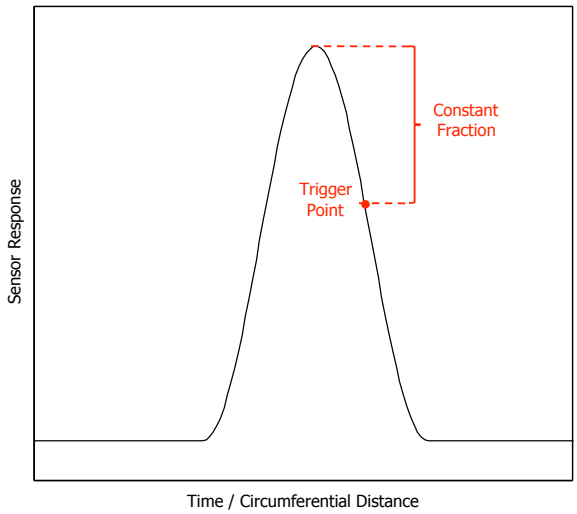

Figure 2.4: Constant fraction crossing ToA definition

is not specified by Von Flotow et al. [21], who use a similar approach.

2.6 Zero Crossing

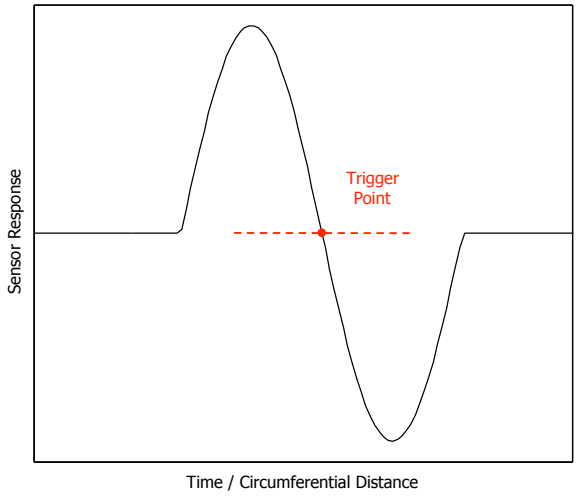

Figure 2.5: Zero crossing ToA definition

As zero crossing assumes a different waveform than the one the optical and non-optical sensors used in this study produce, this ToA definition will be briefly described but not discussed in further detail. However, it is considered a valid approach to ToA

definition and needs to be mentioned in order to give a comprehensive account of the literature.

The waveform used in this approach exhibits a change of sign, and therefore peaks twice, once with maximum of positive sign and once with a minimum of negative sign.

As depicted in Figure 2.5 and described by Heath and Imregun [10], the clock is triggered when the signal crosses the x-axis, thus the designation zero-crossing.

2.7 Discussion

In order to compare and discuss the existing definition, evaluation criteria are chosen: accuracy; computational effort; and versatility.

In the subsequent sections, the ToA definitions are evaluated in these criteria.

2.7.1 Accuracy

In order to accurately measure the ToA of a turbine blade, the sensor should see the blade tip at the moment in time at which the triggering occurs. This means that, assuming a waveform peaking at the maximum response, the triggering should occur close to the peak. If the clock is triggered too early or too late – meaning too far away from the peak – the time measured is not exactly the ToA of the actual blade tip but rather of some point on the blade closer to the center of the disk. If this is the case, certain parameters NSMS seeks to compute cannot be derived with a sufficient degree of accuracy, such as mode, phase, and amplitude of vibration and state of stress of the blade.

Of the approaches described above, the measurement technique of maximum amplitude fulfills this criterion best. Triggering the clock at the very tip of the signal peak means that the blade tip is fully in the field-of-view of the sensor.

The accuracy of the maximum amplitude rate approach highly depends on the waveform. If the amplitude increases most closely to the peak, this technique represents a "highly accurate description"[1]. This might, however, vary with different geometries under investigation, which means that the degree of precision varies as well.

When using fixed voltage crossing or constant fraction crossing for triggering, the degree of accuracy depends on the choice of threshold value or percentage, respectively. It seems that choosing a high threshold or fraction greatly improves precision, however, this can cause serious difficulties in other respects, see Section 2.7.3.

2.7.2 Computational Effort

This section evaluates the computational effort required to determine the exact ToA according to the different definitions.

The ToA approach using a fixed voltage crossing is evidently the simplest one. An absolute value is defined and as soon as the sensor output exceeds this value, the triggering occurs.

The computation to find the maximum amplitude is more complex because the computation needs to take two measurements into account to find the local maximum of the waveform.

The constant fraction crossing technique is a combination of both of the above. The maximum needs to be located, and then the threshold value is computed using a fixed percentage of the maximum value. Once this threshold is crossed, the clock is triggered. Since the maximum response varies from peak to peak, the threshold value must be computed for each peak, which makes the computation more complex.

The ToA approach using the maximum amplitude rate trigger requires the most computation. In order to compare amplitude rates, at least three measurement points

and the change in amplitude between them, must be taken into account for the computation. Other approaches use curve fitting to find the most accurate means for finding the maximum amplitude rate. This is certainly very computation-intensive.

2.7.3 Versatility

This section assesses the versatility of the different approaches. In this context, the term versatility is used with respect to the possible range of blade geometries for which the definitions can still produce reasonable results. Certainly, not all possible geometries can be taken into account. However, looking at the definitions and their underlying assumptions, geometries come to mind that could possibly lead the definitions to imprecise outputs.

Change in Maximum Sensor Response

The first geometric feature that changes the triggering is the tip clearance. Using a disk whose blades are closer to or farther away from the probe changes the maximum sensor response. This can occur in the measurement of a cracked blade which is weaker with regard to tensile forces and thus is elongated. Consequently, tip clearance is reduced and the maximum sensor response is increased.

The approaches using maximum amplitude, maximum amplitude rate, or constant fraction crossing adjust to this change in blade geometry. However, the technique using the fixed voltage crossing does not react to such a change, which results in lower accuracy compared to the other approaches.

Change in Number of Peaks per Blade

Another geometric feature of turbine blades that would require all approaches to be improved is one, that causes the signal to peak more than once per blade.

The approach that most evidently encounters problems in such a case in the maximum amplitude technique. This technique would detect more peaks than blades and output wrong ToA data.

For the same reason, the constant fraction crossing approach would fail if the fraction is chosen too close to the peak. In this case, multiple peaks could also cause multiple triggers per blade passing. Nevertheless, if the fraction is chosen sufficiently far away from the peak, such that it is only crossed once per blade, the approach can still output the correct number of ToAs. Yet, this results in a decrease in measurement precision as described in Section 2.7.1. In addition, this threshold needs to be determined manually based on the waveform and is not self-adjusting.

The fixed value crossing approach encounters an analogous problem. If the value is chosen too high, multiple triggers occur per blade passing, if the trigger is chosen too low, the measurement accuracy deteriorates.

Comparatively simple solutions to these issues are explained in Section 2.8.

A similar problem arises with the maximum amplitude rate approach. Although the point of triggering cannot be influenced manually, depending on the waveform, multiple triggers per blade passing can occur. As opposed to both of the techniques described above, this problem cannot easily be resolved.

2.8 Possible Improvements

As described in the previous section, problems can arise when the blade geometry causes the sensor pulse to peak more than once.

One approach to remedy this issue utilizes the windows calculated for filtering noise as described in Section 1.2.3. These windows which are calculated based on 1/rev time, rotor diameter and blade separation can help to determine which data belongs to a single blade. Knowing that multiple peaks belong to one passing, one peak can

be chosen to represent the ToA.

Another approach relies on the utilization of additional inputs. If for example, the number of blades is provided for the ToA analysis and the number of peaks per blade is constant for all blades, the algorithm can compute the number of peaks that belong to each blade, since the total number of peaks per revolution can be measured.

In either case, one possibility for the maximum amplitude technique is to only utilize the first peak and discard data of later peaks. The same applies to fixed voltage crossing. An alternative for the maximum amplitude technique is to find the highest peak. The constant fraction crossing technique can also detect the highest peak and set a percentage but only use the threshold after the last peak as a trigger.

2.9 Conclusion

All four ToA definitions applicable to this research are investigated with respect to accuracy, computational effort, and versatility.

In the scope of this study, the versatility of the technique is essential, because a variety of different blade geometries are investigated. Regarding the tradeoff between the different techniques, the approach using constant fraction crossing as trigger feature represents the most viable means of ToA definition.

If the threshold is chosen wisely, which improves accuracy, and if only the last peak is considered in case of multiple peaks per blade, which, in combination with the capability of self-adjustment to changes in maximum sensor response improves versatility, this approach provides a good means for ToA definition. At the same time, it only requires a moderate computational effort because it only relies on the detection of a peak.

CHAPTER III

TECHNICAL APPROACH

This chapter presents the technical approach of this research, including the different blade geometries, the types of sensors used and their modes of operation, the experimental setup and the measurement procedure.

3.1 Blade Geometry

Since the signal received is only a function of the type of probe used to acquire it and the geometry of the blade, the signatures of several blade geometries are examined. Sometimes the term IBR is used to refer to the turbine blades. IBR stands for **I**ntegrally **B**laded **D**isk.

This study uses 16 different blade geometries to determine the impact of the different features. It is intended to achieve a range of blade geometries that vary in certain features but do not in others. The chosen features are blade width, blade cross-section, tip geometry, and chord angle.

3.1.1 Blade Width

Blade width determines how much of the blade the sensor detects within its field-of-view for how long. Also, the width of the blade relative to the size of the aperture of the sensor is a very important factor in determining spatial filtering. The blade-width-to-sensor-aperture ratio determines how much of the blade is in the sensor's field of view at a given time. If the blade is thinner than the sensor aperture, both sides of the blade are visible for the sensor, see Figure 3.1. The thinner the blade,

the more of the sides of the blade the sensor can see. These differing measurements are averaged together, which blurs the signal. On the contrary, if the blade is wider than the sensor aperture, both sides of the blade never come into view at the same time. This is expected to improve the accuracy since the sensor can more easily be approximated as a point-like probe when its diameter is smaller than the width of the blade.

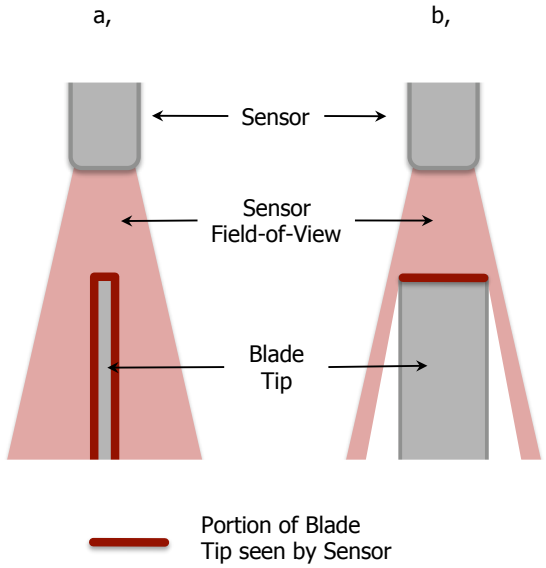

Figure 3.1: Effects of blade width on the measurement: The sensor sees a larger portion of the blade when the blade is thinner than the sensor aperture (a) than otherwise (b)

The range of width of the the blades was determined using a Campbell diagram provided by Pratt & Whitney, see Figure 3.2. A Campbell diagram plots the natural frequencies of the turbine blade and their exciting frequencies versus the rotational speed of the turbine disk. The former relation follows parabolic curves whereas the latter follows straight lines through the origin with slopes equal to the order of vibration, i.e. the number of oscillations per revolution. Resonance occurs at intersections of the parabolas and the straight lines [4]. The minimum width of the turbine blades are determined such that none of the natural frequencies of the blades are excited at the above described resonance freqeuncy. This analysis shows that unless the

thickness is significantly less than 0.1 inches, no resonance occurs over the range of rotational speed of the motor.

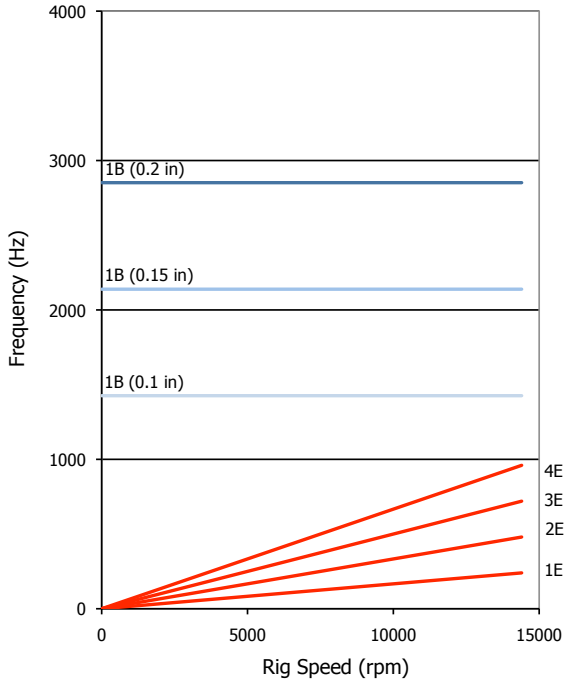

Figure 3.2: Campbell diagram for blade width determination (provided by Pratt & Whitney)

The blade widths are chosen to be 0.1 inches, 0.2 inches, or 0.6 inches. Since the diameter of the microwave probe is much larger than the blade width of the first and second rotor, the resolution of the microwave sensor when measuring the 0.2 inch blade is comparatively low. Consequently, the blade width of the third rotor is chosen to be 0.6 inches, which is larger than the sensor aperture (13.3 mm, 0.52 in).

3.1.2 Blade Cross-Section

Initially, it was intended to keep the geometry of the blades as simple as possible. Consequently, the blades were chosen to have a rectangular cross-section. These blades, however, do not represent real turbine blades very well. Therefore, it was

decided to also investigate blades of varying width. The geometry is still kept simple; the maximum width at mid-blade remains the same as before, but a radius is added, such that the cross-section curves towards a point at its leading and trailing edge. In either case, the cross-section is constant over the length of the blade.

3.1.3 Tip Geometry

The idea of different tip geometries is driven by an invention by General Electric Company: As depicted in Figure 3.3, the blade tip incorporates a so-called Squealer Pocket (United States Patent 6672829). The response of a microwave sensor to such a tip geometry had not been investigated before.

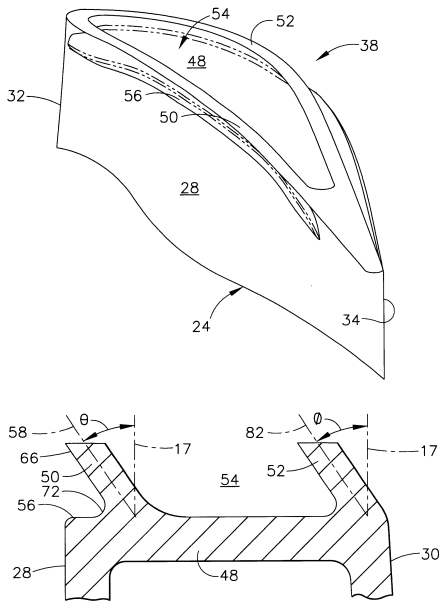

Figure 3.3: Blade tip with Squealer Pocket

A simplified version of such a pocket is integrated into the blade tip of some blades: A thin rim surrounds the pocket on all sides and the pocket always has a depth of 0.1 inches, see Figure 3.4.

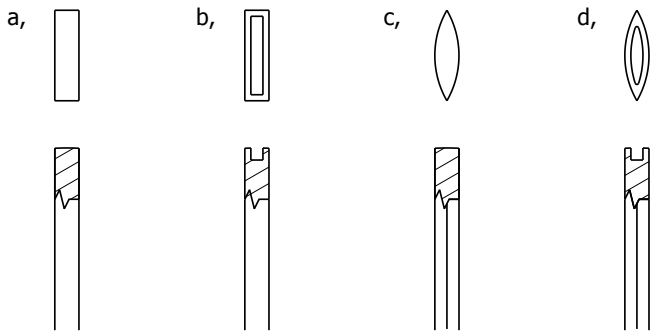

Figure 3.4: Blade geometries, the upper row shows the blade tips, the lower row shows the blades: a) rectangular cross-section, b) rectangular cross-section with pocket, c) varying-width cross-section, and d) varying width cross-section with pocket

3.1.4 Chord Angle

The chord angle is defined as the angle of the radial axis of the disk, which is aligned with the main axis of the turbine, and the axis of the blade at the blade tip. In an actual gas turbine engine, the blade tips are inevitably angled. Since the chord angle has a significant effect on the measurement, it is helpful to understand the impact of this parameter.

In order to approach a more and more realistic blade geometry, the blades on one disk are angled 30°, whereas all other blades have a chord-angle of 0°. The results from conducting measurements on both give a qualitative understanding of the effect of the chord angle.

3.1.5 Experimental Disks

The experimental setup utilizes four different turbine disks. The drawing in Figure 3.1.5 shows one of these experimental disks. They are about 4 inches in diameter

and made of aluminum. These rotors are used to gain fundamental understanding of the interaction between the microwave sensors and the blades.

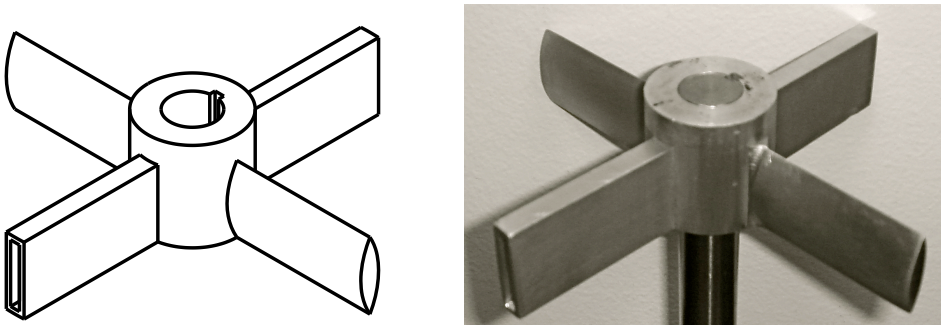

Figure 3.5: Drawing and photograph of experimental turbine disk (blade width 0.2 in, diameter 4 in)

The combination of the features discussed above, leads to 16 geometries described in Table 3.1; the 16 geometries are combined in 4 turbine disks, designated IBR 0.1 in, IBR 0.2 in, IBR 0.6 in, and IBR 0.2 in 30°. All blades of one disk have the same maximum width, for balancing reasons. On each disk, there are two blades with a varying and two blades with a constant width. One of each of the blades of varying and constant width, has a pocket in the blade tip. IBR 0.2 in 30° only differs from IBR 0.2 in in the chord angle.

The blade tips of all turbine blades are polished to improve the reflection of the laser beam used in the optical measurements.

Detailed technical drawings of all turbine disks can be found in Appendix A.

Table 3.1: Overview of blade geometries

	Blade Number	Width [in]			Cross-Section		Blade Tip		Angle [°]	
		0.1	0.2	0.6	constant	varying	flat	pocket	0	30
IBR 0.1 in	1	•			•		•		•	
	2	•			•			•	•	
	3	•				•	•		•	
	4	•				•		•	•	
IBR 0.2 in	5		•		•		•		•	
	6		•		•			•	•	
	7		•			•	•		•	
	8		•			•		•	•	
IBR 0.6 in	9			•	•		•		•	
	10			•	•			•	•	
	11			•		•	•		•	
	12			•		•		•	•	
IBR 0.2 in 30°	13		•		•		•			•
	14		•		•			•		•
	15		•			•	•			•
	16		•			•		•		•

3.2 Microwave Sensors

The non-optical probes used for this research are microwave probes. This chapter gives an overview of the most important features of microwave sensors.

3.2.1 Microwaves and Radar Systems

Microwaves are electromagnetic waves with a range of wavelength from 1 mm to 1 m, which corresponds to frequencies between approximately 300 MHz and 300 GHz. They propagate at the speed of light. Figure 3.6 places microwaves in the context of other electromagnetic radiation.

The microwave sensor used in this research is a phase-based short-range radar system

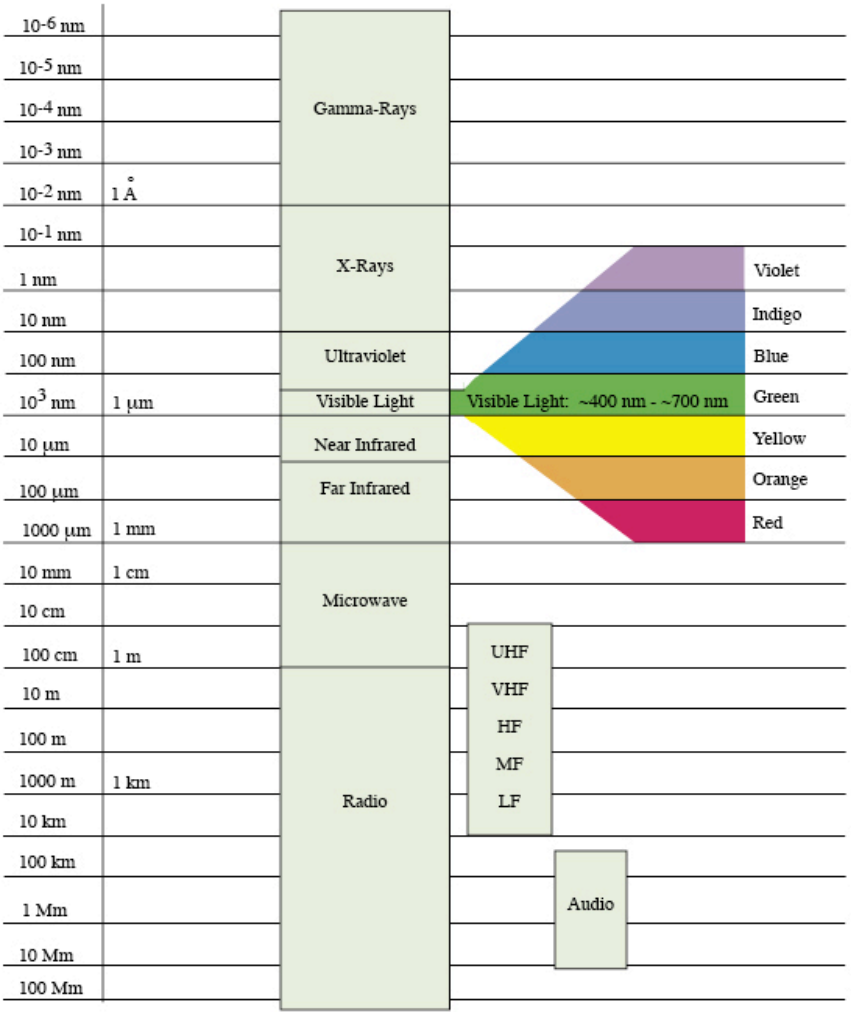

Figure 3.6: Electromagnetic spectrum (the left column gives the wavelengths) [16]

which operates at a frequency of 5.8 GHz; which corresponds to a wavelength of approximately 50 mm (2 in). . Radar is an acronym standing for **Ra**dio **D**etection **A**nd **R**anging. The basic components of radar systems are the transmission, reception and analysis of reflected electromagnetic waves. Conventional long-range radar systems measure the time of flight (ToF) between the transmission of a pulse of radar waves and its reception. The ToF depends directly on the distance the signal traveled, according to Equation 3.1.

$$ToF = \frac{2 \cdot d_{absolute}}{c_{air}} \tag{3.1}$$

c_{air} is the speed of electromagnetic waves in air and $d_{absolute}$ is the distance from the target. This distance is doubled in Equation 3.1 because the radar waves must travel to the target and back. As described by the fundamental radar equation, Equation 3.2, the radar system is able to detect and recognize the energy reflected off the target:

$$P_r = \frac{P_t G^2 \lambda^2 \sigma}{(4\pi)^3 {d_{absolute}}^4} \tag{3.2}$$

where

P_t	power transmitted
P_r	power received back at radar
G	antenna gain
λ	wavelength
σ	radar cross-section of target

As opposed to conventional radar systems, the microwave system used in this research mixes the transmitted microwaves with a reference signal to obtain two channels, Inphase and Quadrature, phase shifted 90°. These two channels determine the phase shift, $\theta_{relative}$, between the reflected and the reference signal. Consequently, the amount of reflected energy, which depends on the radar cross-section (RCS), can be decoupled from phase change, which depends on the distance from the target. The output of the microwave sensor can be represented as a vector, the target vector, $\mathbf{T}$ in the complex plane, where the x-axis represents the Inphase channel and the y-axis represents the Quadrature channel, see Figure 3.7. The target vector can then be divided into radial and phase components. The radial component, which is the RCS,

indicates the amount of energy from the target. The phase component is the phase shift between the reflected and the reference system.

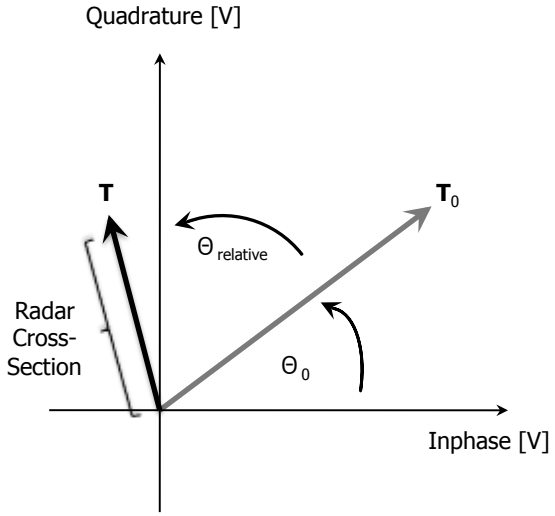

Figure 3.7: Inphase and Quadrature channels plotted in the complex plane

Figure 3.7 describes the measurement as the target moves away from the antenna. First, as the distance between the target and the antenna increases, $\theta_{relative}$ increases. Second, the amount of energy received at the antenna of the sensor decreases as the target moves away, which results in a decrease in RCS. Consequently, the target vector decreases in magnitude and increases in phase. The combination of both of these effects causes the measurement to spiral counterclockwise towards the origin of the coordinate system.

The phase is determined by the distance traveled by the reflected signal relative to the distance traveled by the reference signal at the point of mixing. The phase difference in radians between the two signals can be calculated by Equation 3.3:

$$\theta_{relative} = \theta_0 + mod(\frac{2d_{absolute}}{\lambda_{air}}) \cdot 2\pi \tag{3.3}$$

where θ_0 is an internal system phase, depending on the sensor, $d_{absolute}$ is the distance of the target from the system (half the distance traveled by the signal), and λ_{air} is the wavelength of the microwave in air.

When measuring small variations from a known distance, the number of full wavelengths traveled, n, the internal system phase, θ_0, and the wavelength in air, λ_{air}, are known. If the phase, $\theta_{relative}$ is measured, the absolute distance from the sensor to the target can be calculated by rearranging Equation 3.3:

$$d_{absolute} = \frac{1}{2} \cdot (\frac{\theta_{relative} - \theta_0}{2\pi} \cdot \lambda_{air} + n \cdot \lambda_{air}) \tag{3.4}$$

In this way, the distance between the sensor and the target can be calculated as described by Equation 3.4 and Figure 3.8 [6].

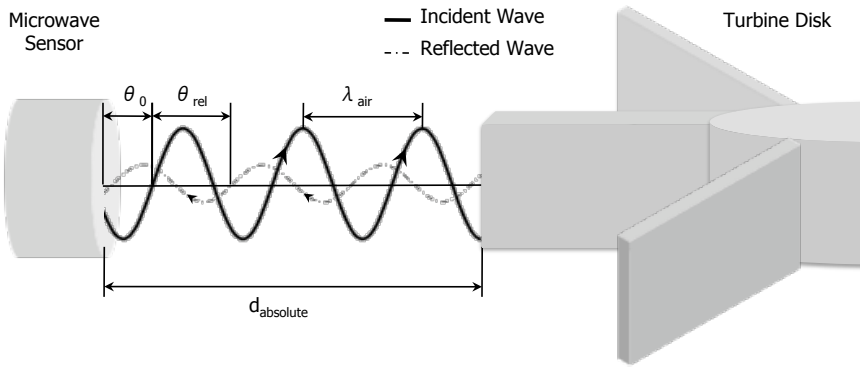

Figure 3.8: Schematic of emission and reflection of microwaves

Further details on the sensor used can be found in [13].

The conversion of Inphase and Quadrature measurements to phase change and thus, distance, which is used for tip clearance evaluation, is very computation-intensive. ToA measurements, however, can be based on the simpler RCS computations. Therefore, this research does not further use the ability of the microwave system to output phase data, but solely relies on the RCS waveforms.

3.2.2 Antennas and Fields

Antennas fulfill the primary function of propagating waves away from a radar system and/or collecting waves and passing them on to a processing unit as electrical signals.

Patterns and Bands

The propagation of waves is not perfectly even in all directions. All antennas exhibit a pattern that describes the power output and reception in every direction; each direction only accounts for a certain amount of the total power of the system. Moreover, microwaves like all electromagnetic waves are directional, or polarized, which influences the antenna pattern. Consider two kinds of antennas; directional and non-directional. In case of a directional antenna, more power is propagated in certain directions, whereas a non-directional antenna sends power out more evenly in all directions. In addition, every antenna is designed to propagate waves of certain frequencies, called the band of the antenna. The range of frequencies in which the antenna can be employed is referred to as the bandwidth.

Fields

The field of an antenna is the region of propagation of the radiation.

The field is approximated to be fairly conical and to have a total angle of aperture of about $45 - 60\,^{\circ}$. This is a matter of convention as there is no defined line beyond which there are no microwaves but they drop off in power as they diverge from the central axis. Moreover, the field is assumed to be asymmetric. The antenna usually propagates more power to one side than to the other. Also, the microwaves will be affected by extremely small tolerances on the mechanical parts of the probe itself which makes it unlikely for the beam to be perfectly symmetric.

This field can be broken down into the far-field and the near-field. The near-field is then subdivided into the radiating near-field and the reactive near-field. Each of

theses fields is characterized by different properties. In the far-field, the propagation of electromagnetic waves is relatively uniform and the wave can be approximated as one-dimensional. For an antenna transmitting waves of wavelength λ and with aperture length D, the far-field is conventionally defined as the region outside of

$$d_{far-field} > \frac{2D^2}{\lambda} \tag{3.5}$$

The radiating near-field exhibits mainly uniform antenna propagation. However, the difference in distance and direction of different points of antenna and target cause complex interactions between waves.

The reactive near-field is characterized by interactions of the antenna and the target which leads to changes of the antenna with respect to the propagation characteristics themselves. Therefore, it is difficult to exactly characterize the field – bringing something close enough to the antenna to measure the field automatically changes the field.

The reactive near-field is the least understood field and is rarely used for normal operation. By convention, the reactive near-field is the region within

$$d_{reactive\ near-field} < \frac{\lambda}{2\pi} \tag{3.6}$$

For the application of microwave sensors for NSMS, the sensors operate well within the reactive near-field.

3.3 Optical Sensors

The optical system used in this study consists of a helium-neon (HeNe) laser and a photodiode. The signal is transmitted to and from the turbine disks through fiber

optics. The experimental setup is explained in more detail in Section 3.5.

Laser

A laser is a device that emits visible electromagnetic radiation through a process called stimulated emission. The term "laser" is an acronym for **L**ight **A**mplification by **S**timulated **E**mission of **R**adiation [9]. Laser light is usually spatially coherent and of a narrow wavelength spectrum, i.e. monochromatic light is emitted in a low-divergence beam. However, the word light is used in a broader sense, referring to electromagnetic waves of any frequency, not only within the visible spectrum. So generally speaking, in addition to lasers emitting radiation in the visible spectrum, there are infrared lasers, ultraviolet lasers and others.

The spectrum of a helium-neon laser like the one used in this study shows the very high spectral purity intrinsic to nearly all lasers, see Figure 3.9. This laser is said to emit waves of a wavelength of 632.8 nm, which is well within the visible spectrum. As the laser beam hits a surface, it is visible as a red spot. To put this laser into context of microwaves and other electromagnetic radiation, please refer to Figure 3.6.

The output of a laser may be continuous or pulsed. This research employs a laser in continuous wave mode of operation; its output is 0.650 mW with a signal to noise ratio of 23.

Photodiode

A photodetector is needed in order to detect the light reflected off of the turbine blade surface. This study utilizes a photodiode.

A photodiode is a type of photodetector in the form of a PN junction or a PIN structure, capable of converting light into either current or voltage. When a photon of sufficient energy strikes the diode, it excites an electron thereby creating a mobile

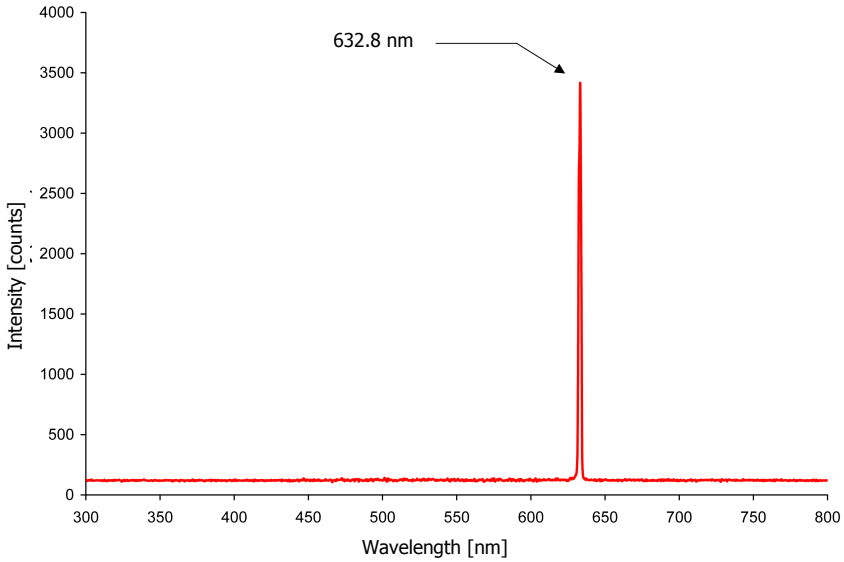

Figure 3.9: Spectrum of a helium neon laser showing the very high spectral purity [22]

electron and a positively charged electron hole. If the absorption occurs in the junction's depletion region, or one diffusion length away from it, these carriers are swept from the junction by the built-in field of the depletion region. Thus holes move toward the anode, and electrons toward the cathode, and a photocurrent is produced. If the reflected wave have traveled a long distance, the energy that reaches the photodiode is lower than if the wave has not traveled as far because of attenuation. Consequently, the converted current or voltage can be directly related to the distance the wave has traveled.

The photodiode used in this study has a rise-time of $< 1\,\text{ns}$ and a spectral range of $200 - 1100\,\text{nm}$. Consequently, the photodiode can detect the HeNe laser light of $632.8\,\text{nm}$.

The setup and mode of operation of the optical system used in this study is given in Section 3.5.

3.4 Spatial Filtering

Filters used in signal processing usually act on one-dimensional signals. Spatial filters, however, are two- or three-dimensional, e. g. an optical circular filter acts to smooth the two-dimensional intensity profile of a laser in a similar way as a low-pass filter acts to smooth an electrical signal.

Moreover, spatial filtering also refers to the "fuzziness" and uncertainty of many-dimensional measurements. Ideally, a dimensional mechanical point measurement would be taken with an infinitesimally small probe tip, the point of contact would be infinitesimal. Realistically however, probes have a finite size. Consequently, errors are introduced because the point of contact is not necessarily the probe tip, as depicted in Figure 3.10. In this case, the point tip takes the shape of a sphere, and the point of contact varies as the measurement is taken. These measurement locations are shown as the dotted line and differs significantly from the original surface. Consequently, accuracy is lost.

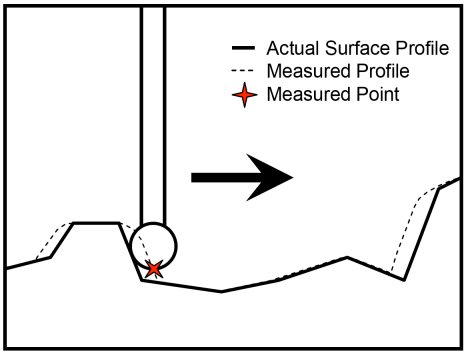

Figure 3.10: Schematic of spatial filtering with a mechanical measurement probe [13]

Spatial filtering also occurs in measurements utilizing non-contact probes. However, the underlying effect causing it is slightly different.

As described by Figure 3.11, the beam of the probe does not converge in a single point. Instead, the area of projection is circular and of finite size. Some amount of the waves

at all locations within this circle is reflected back to the antenna. The reflected waves are vectorially added at the antenna in the form of a weighted integration over the surface within the sensor's field-of-view. The result is a single final signal that is sent to the processing unit and used for subsequent calculations.

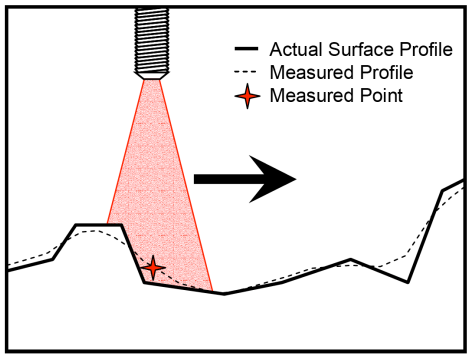

Figure 3.11: Schematic of spatial filtering with a non-contact measurement probe [13]

As can be seen in Figure 3.11, this averaged measurement location can deviate from the actual surface.

3.4.1 Spatial Filtering in Microwave Measurements

In the case of a phase-based microwave sensor like the one used in this study, all reflected waves are approximately of the same wavelength. However, they are different in two other features; the phase shift and the amplitude.

The phase shift of each signal depends only on the distance the signal traveled, which is twice the distance from the antenna to the target. If the sensor takes a measurement on a flat surface, only the point in the center of the field-of-view is at the shortest distance from the antenna, all other points are slightly farther away. In this case, all phase shifts of the reflected waves combine into a single phase shift that is farther away than the ideal point measurement. If the sensor measures an uneven surface,

the weighted average of all phase shifts of the reflected waves shifts the phase of the aggregate to a point that is somewhere in the middle.

The amplitude of the reflected signal is much more complicated because it is influenced by various variables. Amplitude is a measure for the power received back at the antenna and it is a function of attenuation, angle of incidence, angle with the central axis, and surface and material qualities. Attenuation is the reduction in the strength of a signal, in this case the power dissipation as the waves travel through space. For microwaves, attenuation is a function of the distance the wave travels and the atmospheric conditions through which the wave travels. The angle of incidence and the angle with the central axis influence the amount of power that is received back at the antenna. The angle of incidence may cause microwaves to be reflected in such a way, that the reflected wave does not travel back to the sensor. The angle with of the central axis has an impact on the measurements because of non-uniform antenna patterns; the antenna pattern relates the angle with the central axis to the energy transmitted in that direction. Usually, less energy is transmitted at an angle than along the central axis. Consequently, the reflected waves from within the center of the the field-of-view have a greater impact on the overall measurement. Lastly, the surface and material quality govern the amplitude. The surface quality determines the amount of scattering of the reflected waves. A rough surface finishing causes more scattering at reflection than a smooth surface finishing. In this context it is important to note, however, that a rough surface at an angle reflects more waves back to the antenna because of scattering than a smooth surface.

The problem of spatial filtering has been widely investigated. Different approaches to overcome spatial filtering with various sensors have been developed but go beyond the scope of this study. For further information on these approaches for microwave sensors, please see [8] or [18].

3.4.2 Spatial Filtering in Optical Measurements

As described above, spatial filtering occurs when the beam of a non-contact probe does not converge in a single point. However, the field-of-view of a laser beam is so tightly focused onto a surface, such that the area within the field-of-view appears point-like compared to the size of the object under investigation. If the measurements taken over this small area within the field-of-view are averaged, this measured point is very close to the actual surface. The effect of spatial filtering in optical measurements is therefore insignificant and the field-of-view of the laser can be treated as a infinitesimally small point in subsequent calculations.

3.5 Experimental Setup

This Section describes the concept and realization of the experimental setup and the systems of which it consists as well as its range of application.

3.5.1 Concept

The experimental setup used in this research fulfills a particular set of requirements. It is designed to be capable of incorporating a range of different turbine disks, an optical and a microwave system and outputting accurate signals that can be used for analysis.

The basic idea is to arrange the probes around the turbine disk, such that the blade tips will pass them within their active field. In this way, reflections off the passing blades will cause the signal of the stationary probes to vary over time in a repetitive manner. The microwave systems should be able to generate a reliable and reproducible signal. The signal of the microwave probe can be verified by also utilizing an optical probe of higher resolution. Therefore, an optical system is also integrated

into the spin rig.

Since vibrations of the turbine blades are not under investigation, the resonance frequencies of the blades where vibrations are largest must be avoided. Therefore, the rotational rate of the turbine disk must be easy to control. Resonances occur at certain combinations of rotor speed and natural frequencies of the blades. Consequently, it is preferable to have a means of speed control that permits the drive to automatically be run through predetermined speed regimes in order to avoid resonance frequencies. This would also, later on, allow one to target resonance frequencies for further investigation, beyond the scope of this research.

3.5.2 Realization

A spin rig which meets all requirements of this research is successfully designed and fabricated. Figure 3.12 shows a schematic of the experimental setup including the turbine disk.

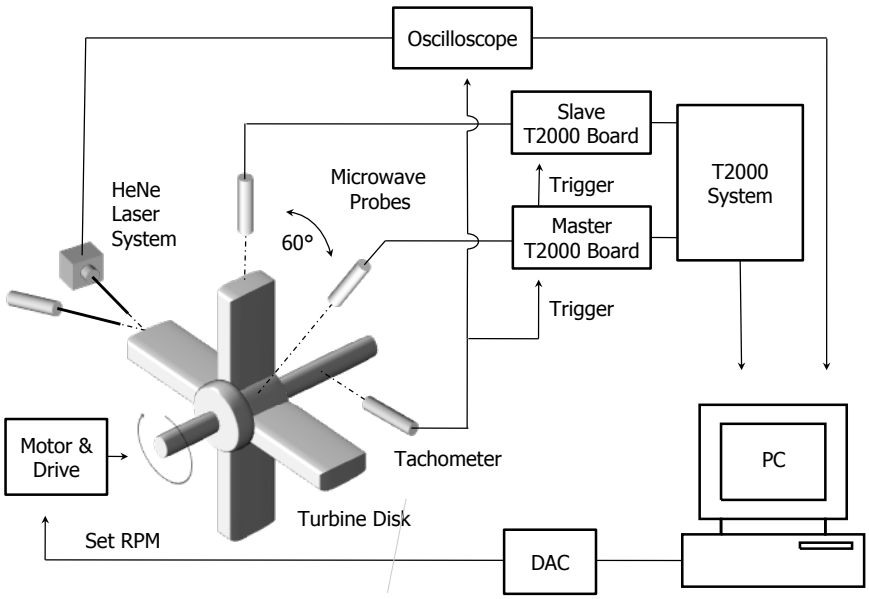

Figure 3.12: Schematic of the experimental setup

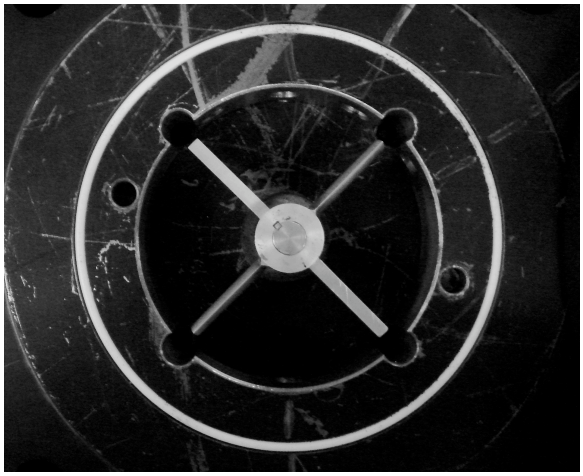

Figure 3.13: Turbine disk (blade width 0.2 in) in experimental spin rig

T2000 Microwave System

The microwave measurements are carried out with the T2000 microwave system by Vibro-Meter. It consists of two microwave sensors, two mainboards and software for signal processing.

The two microwave sensors are facing the turbine blades, spaced at an angle of 60° and are connected to two T2000 microwave blade tip sensing mainboards. An optical tachometer is used as a once per revolution probe to measure the rotation rate of the shaft of the drive. It also triggers the signal of one of the microwave sensors once each rotation. The board of this microwave sensor is the master T2000 system mainboard. It also triggers the signal of the other microwave sensor, which is connected to the slave T2000 system mainboard. In this manner, the two sensor signals are synchronized. The synchronized signals are processed through the T2000 microwave blade tip sensing system and software and are subsequently stored on a computer through an ethernet connection.

Optical Reference System

The optical system consists of a HeNe laser and a photodiode. The light emitted by the laser is transmitted to the surface of the blade through an optical fiber. The optical fiber leads to a probe, see Figure 3.14, which emits the laser light and captures the light reflected off the blade's surface.

Figure 3.14: Optical probe

The reflected light is then also conducted through an optical fiber and received back at the photodiode. The photodiode passes the signal onto an oscilloscope, which is also triggered by the once per revolution probe, and the signal is then stored. The signal acquired with this optical system is used as a reference for the signal acquired with the microwave system and provides a good means for defining the actual ToA of the blades.

The experimental setup of the optical reference system is shown in Figure 3.15.

Frequency Control

Using National Instruments LabView, a waveform is generated and sent to a digital to analog converter (DAC). This DAC controls a speed reference unit, which outputs this waveform as speed reference voltage to the drive. In this way, the drive can be continuously run through different speed regimes that are of particular interest with

respect to the vibrations of the blades.

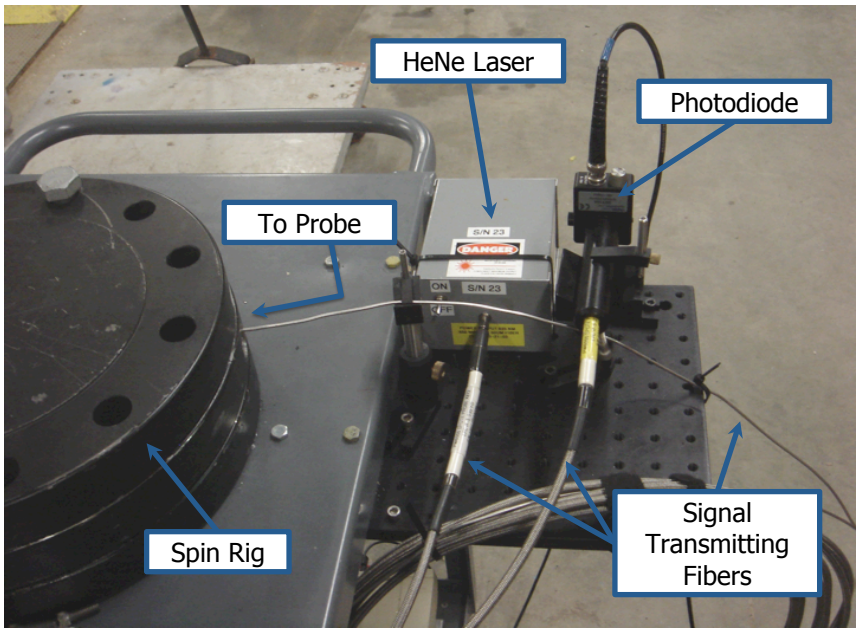

Figure 3.15: Experimental setup of the optical reference system

Field of Application

The construction of this spin rig is designed to be very versatile. Although the blade geometries and the environmental conditions for the tests run in the scope of this research are relatively simple, the rig can also be used to investigate more complex rotors with a wide range of numbers of blades, blade cross-sections or blade materials at low cost compared to large-scale spin testing. In addition, it can be altered to allow for different environmental conditions by changing parameters like pressure or temperature. Also, the spin rig itself is not limited to the types of sensors and their relative position used in this research.

3.6 Measurement Procedure

Dynamic measurements of the ToA involves the following steps:

1. **Initialize T2000 system:** The T2000 mainboards and software are initialized. The software then runs a communication check with both of the microwave probes.

2. **Initialize optical reference system:** The HeNe laser, the photodiode, the oscilloscope and the corresponding software are initialized.

3. **Initialize once per rev probe**

4. **Start LabView and initialize DAC**

5. **Start motor and drive:** The motor and drive are either manually set to a certain number of RPMs (step 4. is not needed in this case) or continuously run following the input data from LabView through the DAC.

6. **Microwave data acquisition:** The measurements using the microwave system are started through the T2000 software, the data is then stored.

7. **Laser data acquisition:** The data from the oscilloscope is uploaded onto the computer and stored.

CHAPTER IV

RESULTS OF MICROWAVE MEASUREMENTS

This chapter presents the results from the microwave measurements. Firstly, the results are analyzed in the time domain. An example of a typical microwave measurement time domain signal is presented and the effects of parameters such as microwave polarization and geometric features of the blades on the time domain signal are investigated. Secondly, the signal is transformed into the frequency domain and it is evaluated whether the findings from the time domain analysis correspond to the findings from the frequency domain analysis.

4.1 Data Acquisition

Using the T2000 software, the microwave signals are acquired. Each signal is averaged over 64 revolutions of the turbine blade.

The explanation of the emission, reflection, and scattering of microwaves presented below is a much simplified approximation of the actual underlying mechanisms. These mechanisms are much more complex since the form of scattering of electromagnetic waves depends on the relative magnitude of the wavelengths compared to the size of the scatterers. In contrast to light, the microwaves emitted by the sensor have wavelengths larger than the blade tip dimensions; the measurements are sub-wavelength. The explanation is intended to facilitate the understanding and interpretation of the microwave data.

As the probe emits microwaves, these microwaves are reflected off the surface of the target, in this case the turbine disk. The microwave sensor response is a measure

of the distance from the target and the power of reflected microwaves detected at the antenna. There are three predominant effects that govern the power of reflected microwaves: attenuation, absorption, and reflection: Firstly, as microwaves travel a certain distance through a medium, the amplitude of the waves decreases with increasing distance – the waves are attenuated. Secondly, as the microwaves hit the surface of the target, a fraction of the power of the microwaves may be absorbed by the material depending on the material properties of the target. Since all rotors used in this study are made from aluminum, the absorption of the microwaves will be equal in all measurements. Thirdly, the angle at which the microwaves hit the surface of the target causes them to be reflected. The direction of the emitted waves is a function of the angle of the incident waves. As a result, depending on the angle of the incident waves, the microwaves may be reflected directly back to the antenna or in another direction such that the reflected waves cannot reach the antenna. Even a small deviation of the direction of the reflected waves from the direction to the antenna will cause the reflected waves to miss the antenna if the distance from the target to the antenna is large.

Consequently, the strength of the signal of microwave output decreases with increasing distance from the target. Therefore, the intensity of the microwave signal rises as the blade moves into the sensor's field of view, reach its maximum as the blade tip is closest to the sensor and then drop again as it moves out of the sensor's field of view. Figure 4.1 shows the typical sensor response to the experimental turbine disks, in this case IBR 0.2 in. Figure 4.1 plots the sensor response to one rotation in analog to digital converter (ADC) counts over time or rotational distance.

Figure 4.1 shows the sensor response measuring one revolution of a four bladed turbine disk. Hence, the signal rises four times. When the signal strength is low – between the peaks – the turbine blades are not within the sensor's field-of-view. This area in Figure 4.1 represents the microwave measurements taken on the core of the rotor

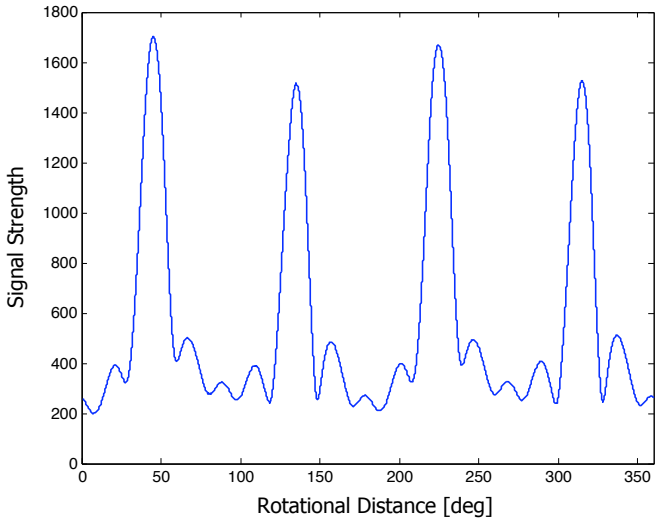

Figure 4.1: Typical sensor response to one revolution of a four-bladed disk

between two turbine blades.

The difference in the response to each blades is explained in the subsequent sections. With very high spatial resolution, the response of the sensor should be a square function, reaching its maximum as the probe sees the passing blade tip and its minimum as the blade is not in the sensor's field of view. As seen in Figure 4.1, the actual signal exhibits a finite rise and fall time, as the blade moves toward and away from the microwave probe. In addition, the signal is pointed instead of flat as the maximum is reached. Both effects are due to spatial filtering of the microwave probe caused by the large spatial aperture of the microwave probe in comparison to the blade width.

4.2 Blade Identification

As described in Section 3.1, each IBR has four geometrically different blades to which the microwave sensor responds differently. For an overview over blade geometries and dimensions refer to Table 3.1. In order to understand how blade tip geometry affects the sensor response, it must be considered which of the four peaks the sensor measures for each revolution corresponds to which of those four blades.

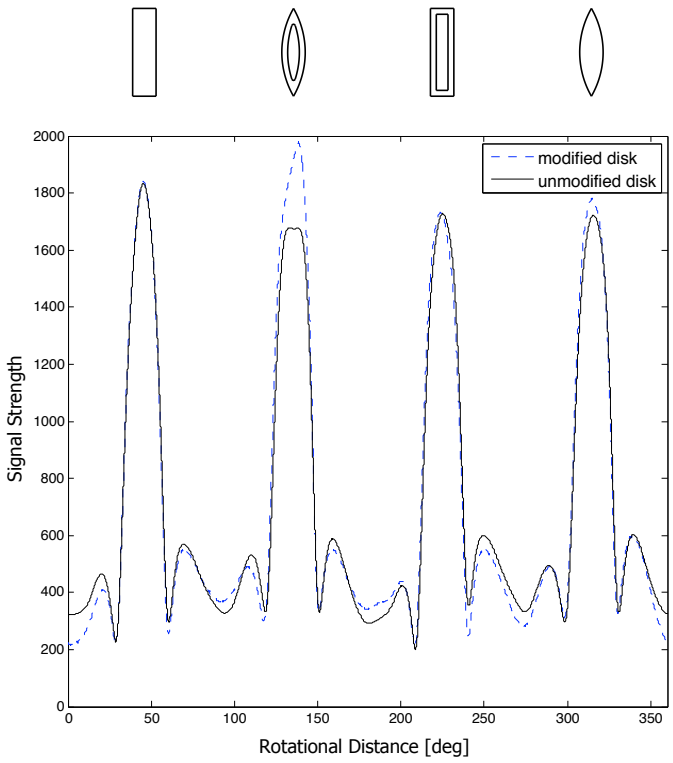

Figure 4.2: Measurements for blade identification

To gain this knowledge, the geometry of the blade tip of one blade is modified with aluminum foil. The modified blade tip is expected to cause a stronger microwave response than the unmodified one. Therefore, measurements are conducted on the modified turbine disk and the unmodified disk. This makes it possible to identify this blade.

The blade which is modified is the one with varying width and a pocket in the blade tip. Aluminum foil is attached at the end to make the blade wider and cover up the pocket. This procedure is conducted on all turbine disks and the results are presented in Figure 4.2 with the IBR 0.6 in as a typical example. Once this blade is identified, the others can be identified as well taking into account the order of the blades in the direction of rotation.

The schematics above the respective peaks in Figure 4.2 indicate which blade tip geometry can be associated with the peak. These schematics are taken from Figure 3.4,

which shows the geometries of all four turbine blades and their blade tips of the IBR 0.2 in.

The data used for the identification of blades on the other turbine disks can be found in Appendix B.

4.3 Investigation of Microwave Polarization

As described in Section 3.2.2, the microwaves in the field-of-view of the sensor are polarized. The direction of polarization has a significant impact on the measurement quality.

If the direction of polarization is perfectly aligned with the axis of the blade at the blade tip, they create a large overlap which results in a large effective area – see Figure 4.3. Vice versa, if the direction of polarization and the blade axis are not well aligned, the effective area is small.

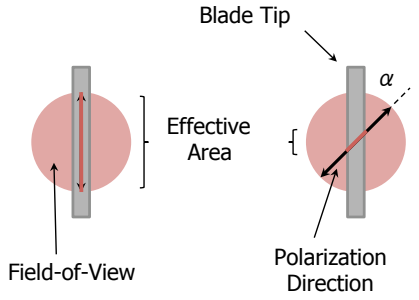

Figure 4.3: Schematic of microwave polarization

Figure 4.4 shows the effect of the polarization on microwave measurements. These measurements are taken on the IBR 0.2 in, which has no chord angle. The microwave sensor is rotated in 45° increments before the measurements are taken.

The more the direction of polarization deviates from 0° or 180°, the weaker the sensor response gets. The peak caused by the blade passing decreases in size, and is harder to identify. The impact that this loss in measurement quality has is obvious – if the

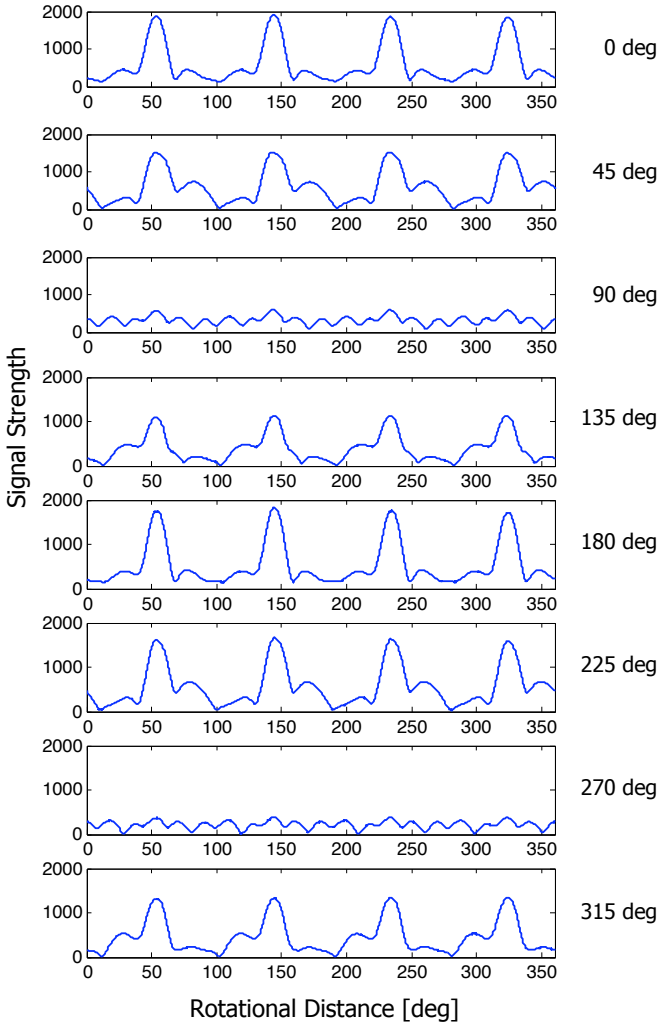

Figure 4.4: Impact of the direction of microwave polarization on measurements. The column on the right states the angle between the direction of polarization and the blade axis

peak caused by blade passing cannot be clearly identified, the objective of measuring the blade tip time of arrival cannot be fulfilled.

Therefore, for all measurements taken in this study, the direction of polarization is well aligned with the axis of the turbine blades with a chord angle of 0°. For the blades with a chord angle of 30°, the direction of polarization and the axis of the turbine blade at the blade tip draw an angle of 30°.

4.4 Impact of Geometric Features

This chapter presents the results from the investigation of the impact of geometric features of the turbine blades on the microwave measurements. The geometric features discussed in this chapter include cross-section, tip geometry, blade width, and chord angle. As described in Section 3.1, these are the features in which the blades differ.

4.4.1 Effects of Cross-Section & Tip Geometry

Figure 4.5 shows the microwave sensor response to one revolution of all experimental turbine disks.

The first thing to notice is the variation in the amplitude of the signals. This section explains how changes in geometric parameters among blades of the same rotor affect the amplitude of the signal. How differences in geometric parameters between rotors, such as blade width and chord angle, affect the signal is described in subsequent sections.

In order to evaluate the data, it is essential to understand the relation between these geometric features and the amplitude of the signal. As the incident microwaves reach the surface of the rotor, the waves are reflected. Depending on the angle of incidence, a portion of the microwaves are reflected back to the antenna and the rest of the microwaves is reflected in other directions. The larger the surface area of the target within the field-of-view of the sensor and the closer to the antenna, the more microwaves are reflected and the more microwaves, thus more energy, can be detected at the antenna. The amplitude of the signal corresponds to this amount of energy received at the antenna.

The manner of representation used in Figure 4.5 makes it easy to compare the patterns of each individual signal: First of all, it is important to notice that the blades of

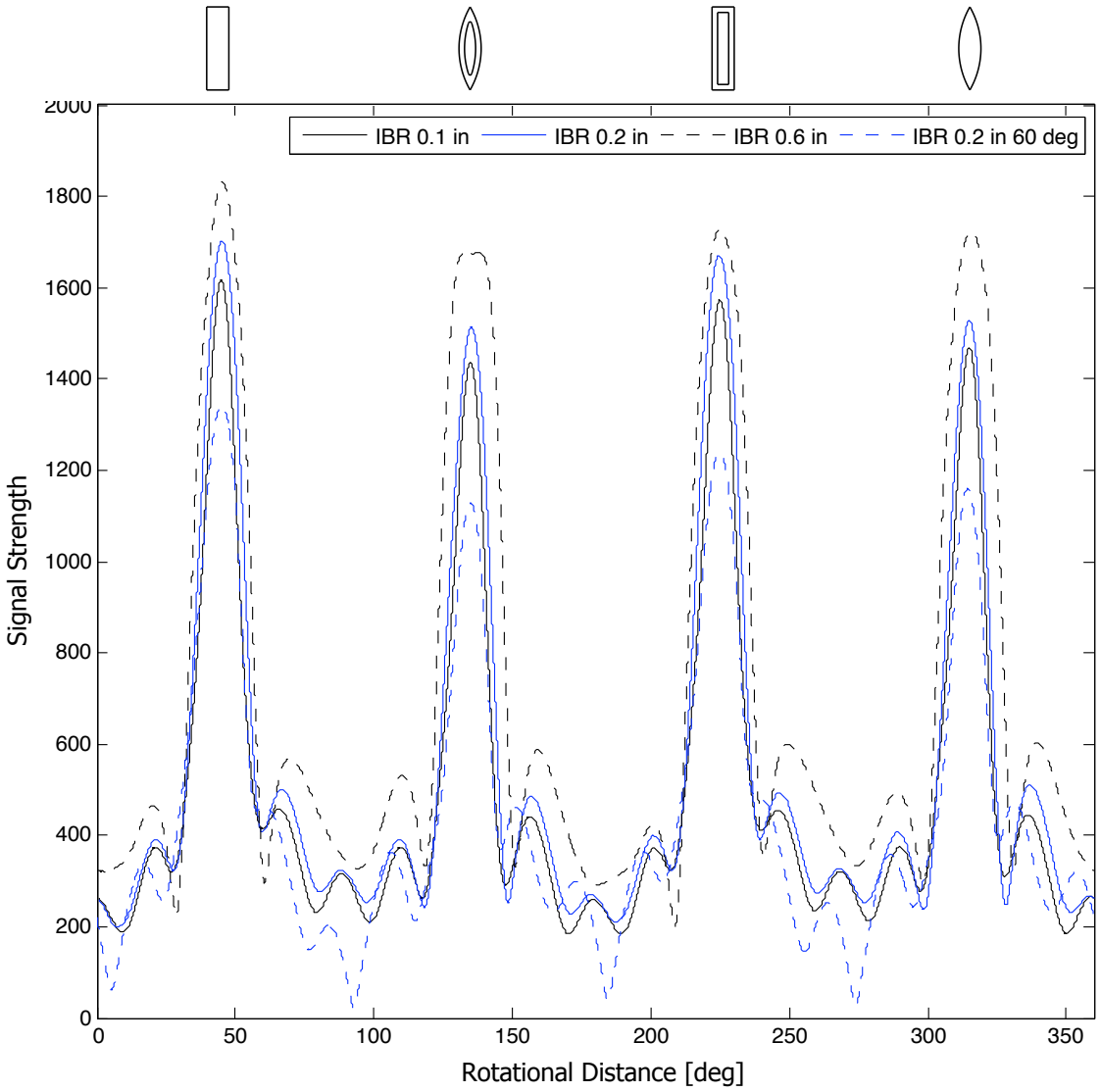

Figure 4.5: Effects of cross-section and tip geometry on the measurement

rectangular cross-section without a pocket in the blade tip cause the strongest sensor response. This applies to all disks independent of blade width or chord angle. This result is not surprising since this tip geometry is expected to cause the least scattering of the reflected microwaves. In addition, because the blade tips of constant cross-section have the highest surface area at minimum clearance of all tip geometries, more energy is reflected back to the antenna.

The weakest sensor response is caused by the blades of varying cross-section with a

pocket. The reasons are the same as stated above – the surface area at the tip is smallest due to the varying cross-section as well as the pocket and the pocket also causes scattering of the reflected microwaves. Consequently, less energy is received back at the antenna.

The same applies to the blades with either varying cross-section or pocket. Here it can be noted, however, that the blades of constant cross-section with blade pocket cause a stronger sensor response than those of varying cross-section without blade pocket. This result can also be shown in the sensor response to all four turbine disks. According to these results, the tip geometry and cross-section features can be ranked with respect to the extend of their impact on the microwave measurements. Differences in the shape of the cross-section affect the sensor response more significantly than pockets in the blade tip.

Although changes in tip geometry and cross-section can be recognized as changes in the signal, only the amplitude of the signal is affected. With one exception, the shape of the waveform apart from the amplitude does not shed light on the geometry of the respective turbine blade. However, the peak caused by the 0.6 inch wide turbine blade with varying cross-section and pocket differs from the other peaks. Either parameter alone does not cause a notable difference in the waveform, but the combination of both causes the peak to be wider and less pointed at the top. Please see the subsequent section for further explanations of this observation.

4.4.2 Effects of Blade Width

Two possible effects caused by differences in blade width include the overall height of the peaks of the signal, and the width of the peaks.

From Figure 4.5 it can be seen how the width of the blades affects the height of the peaks in the sensor response. This effect follows a simple pattern – the widest blade

causes the highest peak and the thinnest blade causes the smallest peak. Analogously to the differences in blade width, the differences in peak height between the 0.2 and the 0.6 inch blades are greater than the differences between the 0.1 and the 0.2 inch blades.

The underlying effect is described in Section 4.4.1: Wider blades have a higher surface area within the field-of-view of the microwave sensor. Therefore, more microwaves are reflected on the surface and more energy is received at the antenna which causes a higher amplitude of the peaks corresponding to the wider blades.

In this analysis, only blades with the same chord angle can be compared since a chord angle unequal to 0° or 180° significantly influences the sensor response and greatly decreases the signal strength, as explained below in Section 4.4.3.

The width of the peaks cannot be evaluated with the manner of representation used above. In order to determine how differences in blade width affect the width of the peaks, the strength of the sensor response must be taken out of the equation. Therefore, the sensor response is normalized for each blade individually. In this manner, the width of each peak can be compared and it can be determined whether the sensor response when not normalized is genuinely wider or just appears so because it is stronger.

Figure 4.6 depicts the sensor response one blade tip geometry and cross-section at a time, which is represented by the schematic in the upper left corner of each plot. The schematics indicate which blade tip geometry can be associated with the peak. These schematics are taken from Figure 3.4, which shows the geometries of all four turbine blades and their blade tips of the IBR 0.2 in. The blades in each plot only differ in blade width and chord angle.

It can be seen that blades of different width cause peaks of different width in the microwave sensor response signal. The signal starts to rise as the respective blade moves into the field-of-view of the sensor and drops again as the respective blade

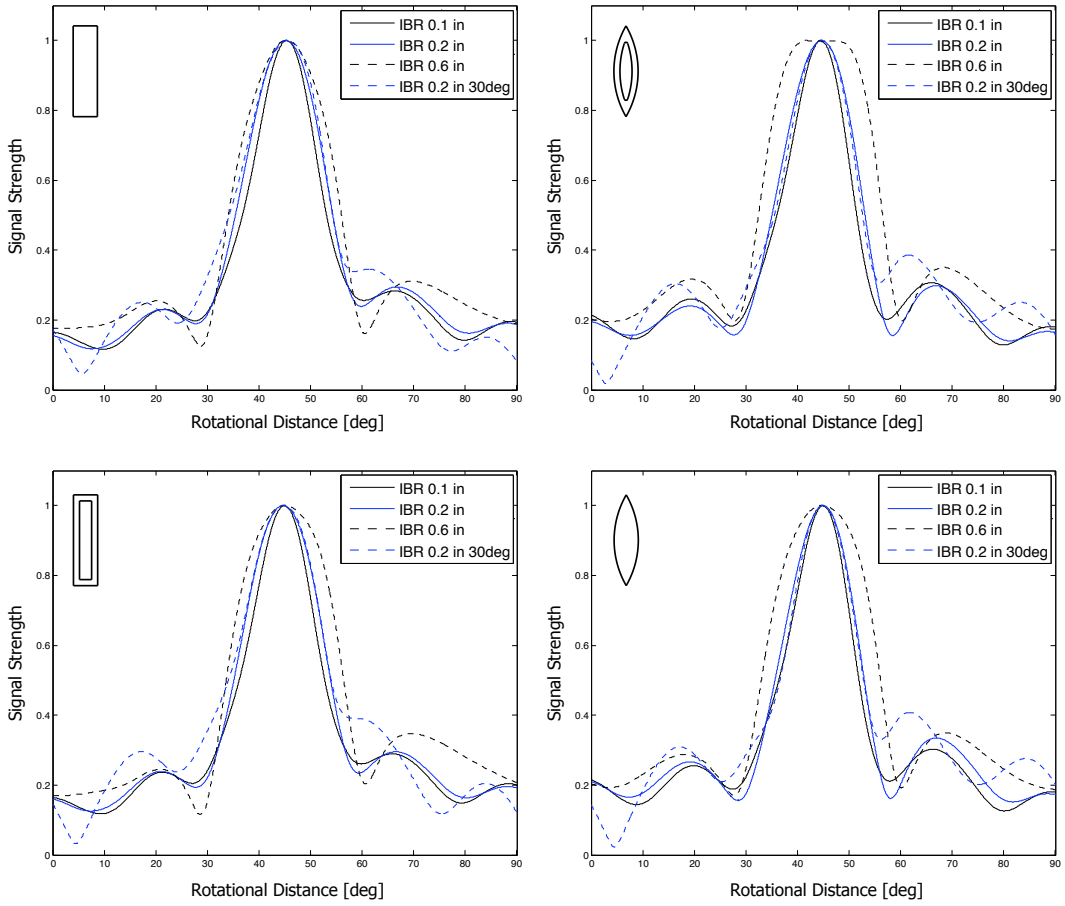

Figure 4.6: Effects of blade width on the measurement

moves out of the field-of-view. With increasing width of the blade, the blade moves into the field-of-view earlier and leaves it later – the blade is detected earlier and for a longer period of time. Consequently, a wider blade results in a wider peak of the signal.

As seen in Figure 4.6, the widest blades, 0.6 inches, indeed cause wider peaks in the sensor response. This result is independent of other blade geometry features such as tip geometry, cross-section and chord angle. The 0.2 inch blades, angled at 30° or without chord angle, cause peaks of approximately the same width. The peaks corresponding to the 0.1 inch blades are the most narrow. It can again be shown that analogously to the differences in blade width, the differences in peak width between

the 0.2 and the 0.6 inch blades are greater than the differences between the 0.1 and the 0.2 inch blades.

As described above, the sensor response to the 0.6 inch blade with a varying cross-section and a pocket in the blade tip carries some information about the blade geometry. This can be explained by the blade-width-to-sensor-aperture ratio. This ratio is largest for the 0.6 inch blades. Thus, the extent of spatial filtering is not quite as influential on these blades as in the thinner blades. The sensor response on these blades provides no insight into the tip geometry because all information is filtered out.

4.4.3 Effects of Chord Angle

The chord angle predominantly affects the measurement in two ways – by changing the length of time during which the blade is in the field-of-view of the sensor, see Figure 4.7, and by changing the angle between the polarization of the sensor and the axis of the turbine blade.

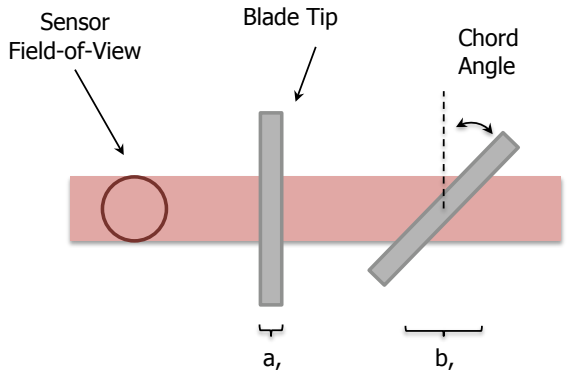

Figure 4.7: Effects of chord angle on the measurement: The sensor traces a longer line across the blade when it is twisted (b) than otherwise (a)

The first major difference between the blades with and without chord angle occurs when the blade moves into and out of the sensor's field-of-view. The angled blade needs more time to enter and leave the field of view.

Consequently, the angled blade causes a wider base of the peak, see Figure 4.6. As

soon as the blade is completely within the field-of-view, the blade angle does not affect the width of the measurement peak.

The second major difference due to the chord angle is found in the overall signal strength. A chord angle of 30° draws an angle of 30° between the polarization of the microwaves and the axis of the blade tip and thus decreases the effective area, see Figure 4.3. Consequently, the response of the microwave sensor is weaker. This effect can be expected when the signal is compared to the measurements taken in the influence of the polarization investigation, Section 4.3. Section 4.3 investigates the effect of an angle between the direction of polarization and the blade tip by rotating the microwave sensor in 45° increments. Although in this section, the blade is angled at 30° and the microwave sensor is not turned, the measurement geometry is comparable since the relative angle between the direction of polarization and blade tip axis is comparable. Please see the measurement taken at 0° and 45° in Figure 4.4 and compare it to the sensor response to a turbine blade with a chord angle of 0° and 30° in Figure 4.5

4.5 Frequency Domain Analysis

Following the analysis of the signal in the time domain, this section presents the findings of the frequency domain analysis.

4.5.1 Discrete Fourier Transformation

The discrete Fourier transform (DFT) is calculated using a fast Fourier transform (FFT) algorithm. For further information on discrete-time signal processing please refer to [19].

DFT of Signal over one Revolution

The signals are windowed with a rectangular window that contains all four peaks.

The sampling frequency at which the signal is acquired is 239970 Hz. This number is caused by the rotational speed of 720 rpm and the fixed number of data points, 39995, per two rotations. Figure 4.8 shows the resulting DFT.

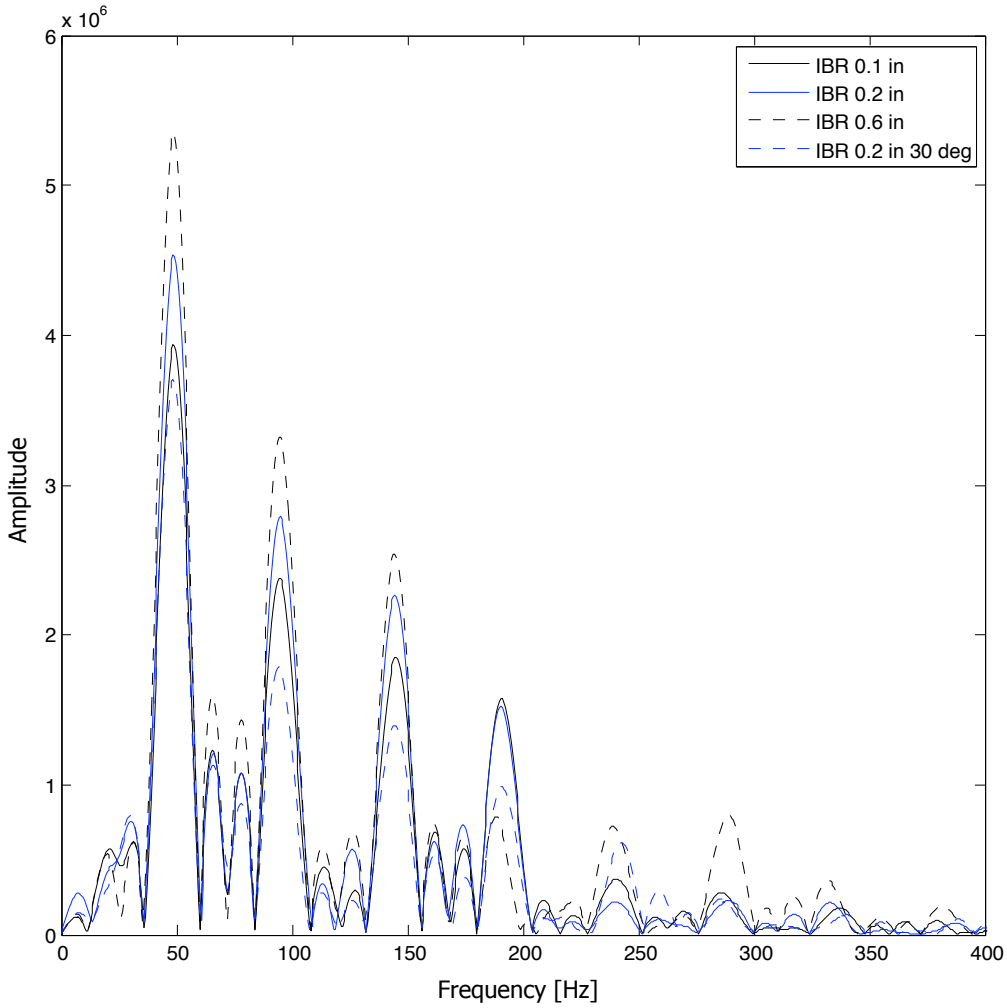

Figure 4.8: DFT of signal over one revolution

The first significant peak occurs at a frequency of 48 Hz, which corresponds to the frequency at which the blades pass the sensor. The next lower peaks occur at multiples of 48 Hz.

The relationship between the amplitude of the peaks and the blade width are consistent with the findings from the time domain analysis of Section 4.4. Amplitude

qualitatively increases with blade width. However as opposed to the time domain results, the difference in blade width is not proportional to the difference in amplitude. Also, the signal of the blade with a chord angle causes the lowest amplitudes.

What causes the two minor peaks that can be found between each pair of major peaks is investigated using a synthetic signal in Section 4.5.3.

Looking at the DFT, no eigenfrequencies can be detected. This conforms to the findings from the Campbell diagram analysis in Section 3.1.1, which show that no eigenfrequencies are excited at this low rotational speed.

DFT of each peak

To see how the geometry of each blade affects the DFT, the signals are windowed with windows that contain only one peak.

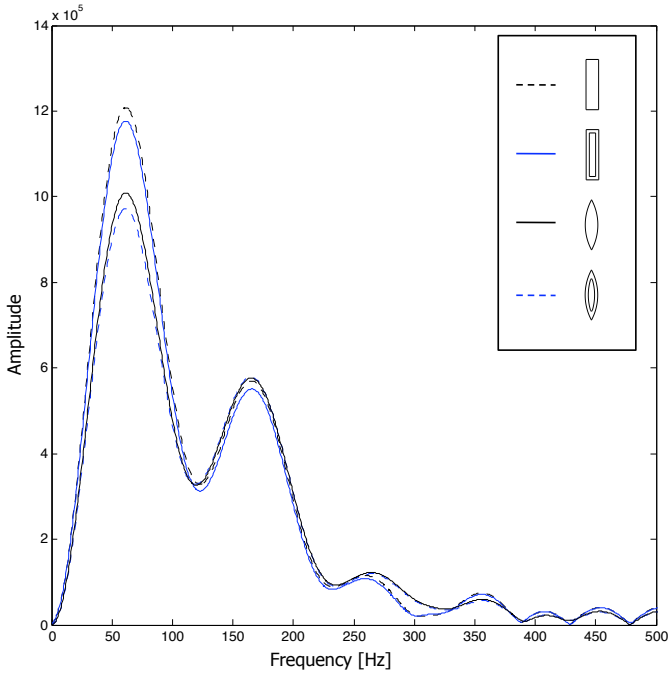

Figure 4.9: DFT of signal over one blade for all four blades separately

Again, the relationship between the amplitude of the peaks and the blade tip geometry and cross-section is consistent with the findings from the time domain analysis.

Figure 4.9 shows the DFT of each blade of the IBR 0.1 in separately. The variation in cross-sectional width causes the amplitude to decrease significantly. The pocket in the blade tip slightly decreases the amplitude further compared to the peaks corresponding to blades without pocket.

The only inconsistency is that the first peak does not occur at 48 Hz. This is investigated in a subsequent section, see Section 4.5.3.

4.5.2 Short-Time Fourier Transformation

In order to investigate how frequencies change over time, the signal is short-time Fourier transformed (STFT). Figure 4.10 plots the frequencies over the time for one revolution at 720 rpm of the 0.1 inch blade. The colorbar indicates the amplitude with which these frequencies occur.

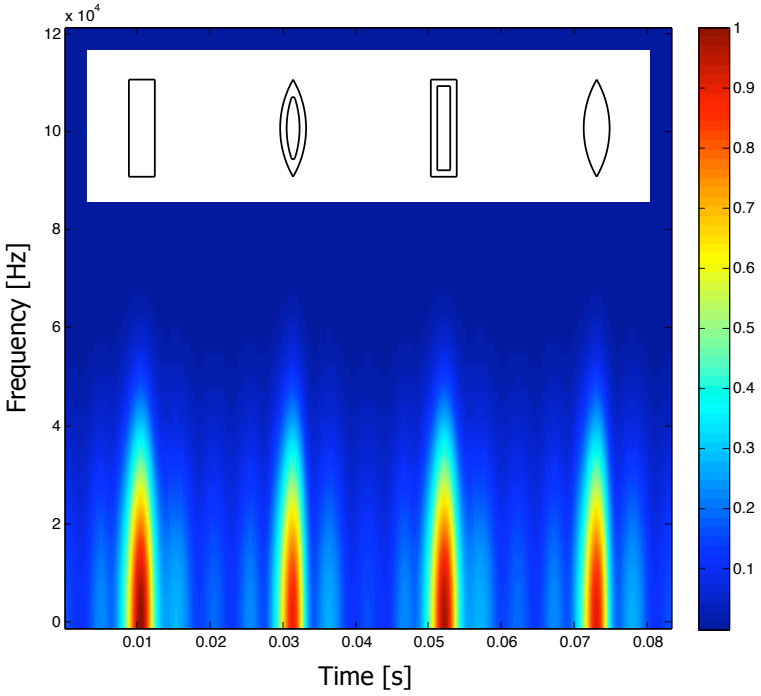

Figure 4.10: STFT of signal over one revolution

Again, it can be seen that the blades with constant cross-section cause frequencies

to occur at higher amplitudes than the blades with varying width. The change in amplitude due to the pocket is slightly present but difficult to detect because of the minimal variation in color.

The STFT analysis also shows that the frequencies occur for a longer period of time for time domain signals of wider blades. Moreover, the chord angle causes the frequencies to occur earlier – the area in the STFT corresponding to the blade passing is stretched and blurred to the left. Please refer to Appendix C for the corresponding plots.

4.5.3 Comparison with Synthetic Signals

Synthetic signals similar to the acquired data are generated in order to better understand the results from the Fourier transformations.

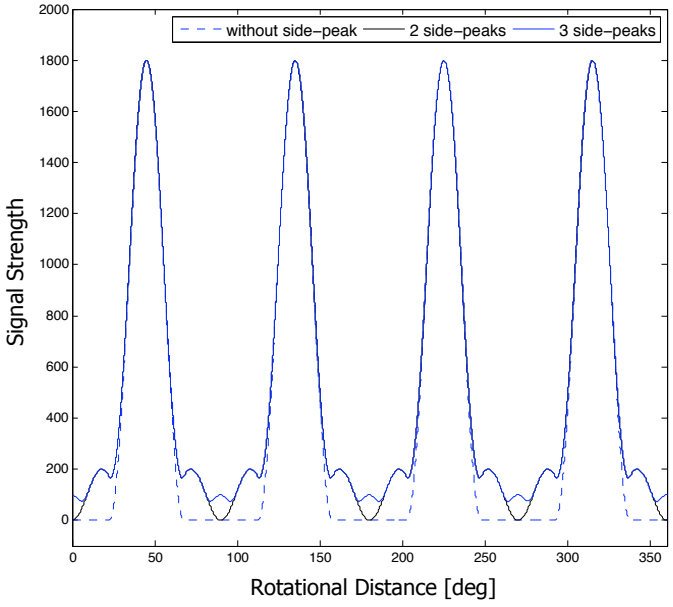

Figure 4.11: Synthetic signal simulating one revolution

The signal is based on a sine function with the frequency of the acquired signal, 48 Hz, simulating the blade passing the sensor, see Figure 4.11. To better approximate the acquired waveform, additional sine peaks are added. These more complex signals are

used to gain better insight in the effect of these additional side-peaks.

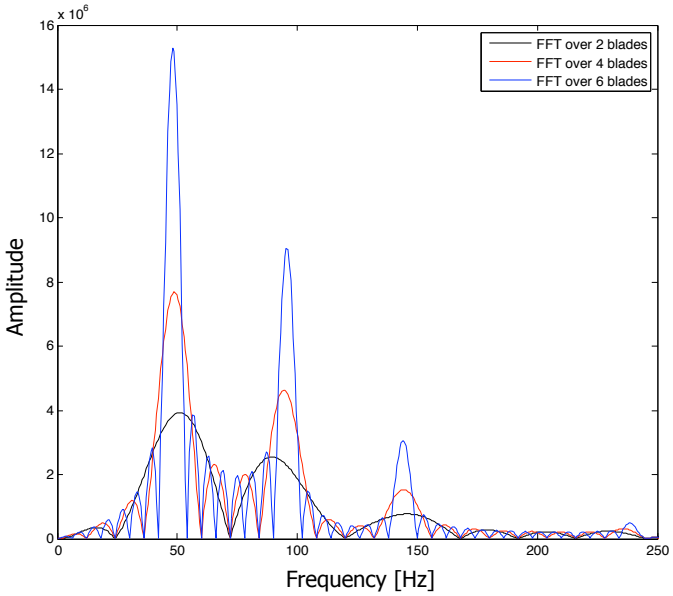

Figure 4.12: DFT of synthetic signal over one revolution

Firstly, the signal is fast Fourier transformed as before, but the window is varied. Since all peaks in the time domain signal are exactly the same, this should not affect the DFT. Figure 4.12 shows the DFT for a window containing 2, 4, or 8 time domain peaks of the synthetic waveform without side-peaks.

The relative amplitudes and absolute frequencies of this DFT correspond well with those of the DFT of the acquired signal. In addition, it appears that the two minor peaks that can be found between each pair of major peaks in Figure 4.8 are leakage due to windowing.

As a second step, all three synthetic signals are fast Fourier transformed using a window containing only one time domain peak. The DFT is shown in Figure 4.13.

It can be noted that the first peak shifts to the right, away from the 48 Hz, compared to the DFT over the signal for one entire revolution. The same phenomenon was observed in the DFT of the acquired signal. Furthermore, it can be seen that the time domain side-peaks only affect the magnitude of the frequency domain peaks but

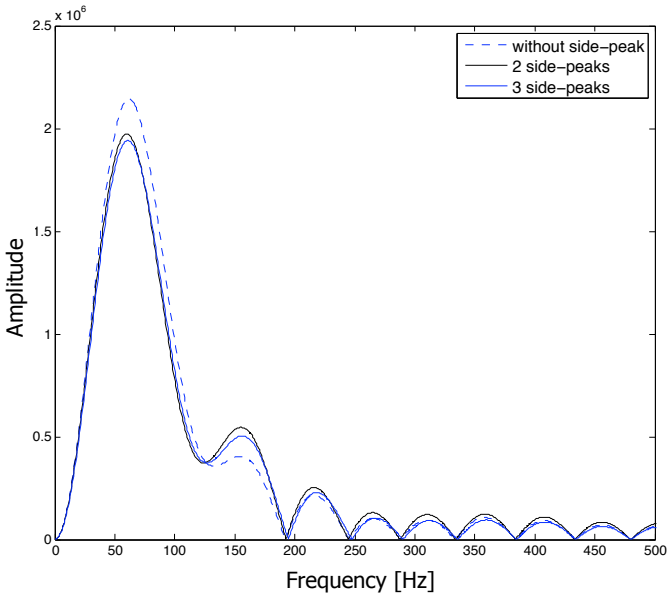

Figure 4.13: DFT of three synthetic signals over one blade

do not cause significant peaks at additional frequencies.

CHAPTER V

RESULTS OF LASER MEASUREMENTS

The optical system is built in addition to the microwave system as a benchmark reference. For years, optical sensors have been used to assess airfoil stress conditions through blade ToA measurements during developmental testing of gas turbine engines. These optical probes provide a characteristically small active area, which enables the timing of a passing airfoil to be resolved with a high degree of accuracy. Therefore, the optical system provides an accurate means for defining the ToA of the blades. The ToA defined with the optical system can then serve as a reference for the ToA definition based on the measurements from the microwave system.

This chapter presents the results from the HeNe laser measurements. Firstly, the results are analyzed in the time domain. Secondly, the signal is transformed into the frequency domain and it is evaluated as to whether the findings from the time domain analysis correspond to the findings from the frequency domain analysis and the results of the microwave measurements.

5.1 Data Acquisition

The laser signals are acquired using the optical setup described in Section 3.5. Each signal is averaged over 128 revolutions of the turbine blade.

As the probe emits laser light, this light is reflected off the surface of the target, in this case the turbine disk. A portion of the reflected light travels back to the probe, and through the optical fiber to the photodiode. The photodiode response is a measure of the energy of the reflected light detected.

The energy of the reflected light is a function of the angle of reflection, which depends on the surface quality – a smooth surface causes the reflected light to be scattered less than a rough surface.

Even slight scattering due to the reflection on slightly rough surfaces at a larger distance from the probe leads to a less amount of energy detected, because even a small deviation of the direction of the reflected light from the direction to the probe will cause the reflected light to miss the probe if the distance from the surface to the probe is large.

Therefore, a large portion of the incident light is reflected back to the probe when the light hits the polished surface of the blade tips. On the contrary, the unpolished, comparatively rough surface of the sides of the blades, the rotor core, and the pockets cause the reflected light to be scattered more, thus less of the reflected light reaches the probe and can be detected. Consequently, the signal rises as the turbine blade moves into the field-of-view and falls as the laser spot leaves the blade tip either because the blade has passed the probe or because the laser spot moves into the pocket of the blade tip.

Figure 5.1 shows the sensor response measuring one revolution of the IBR 0.2 in. The microwave sensor response to the same IBR is also plotted for reference.

Because the sensor sees four turbine blades per rotation, the signal rises four times. When the signal strength is low – between the peaks – the turbine blades are not within the sensor's field-of-view. This area in Figure 5.1 represents the laser measurements taken on the core of the rotor between two turbine blades.

The difference in the response to each blade is explained in the subsequent section.

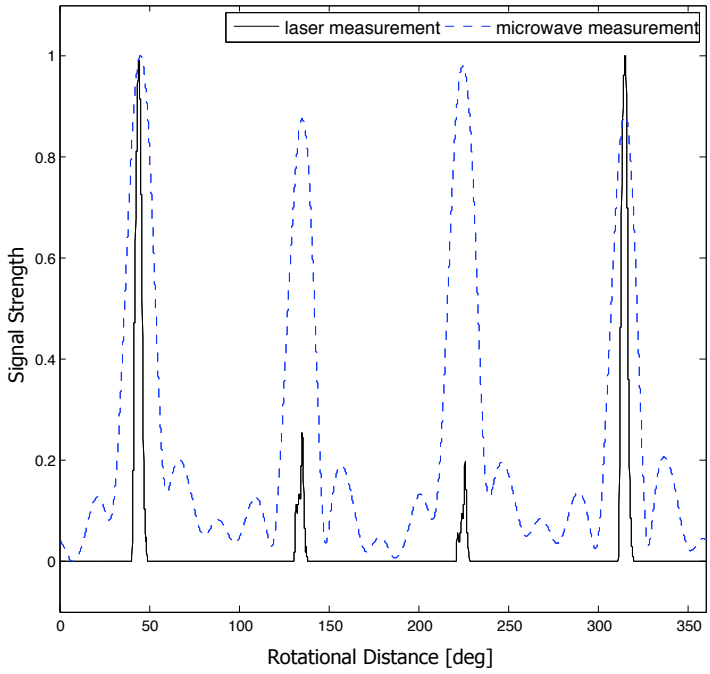

Figure 5.1: Typical optical sensor response to one revolution of a four-bladed disk. The microwave response to the same IBR is plotted for reference

5.2 Blade Identification

As described in Section 3.1, each IBR has four geometrically different blades to which the laser responds differently. For an overview over blade geometries and dimensions refer to Table 3.1. In order to understand how blade tip geometry affects the sensor response, it must be considered which of the four peaks the sensor measures for each revolution corresponds to which of those four blades.

The procedure described in Section 4.2 is not required for the laser measurements to identify the blades. Due to the high resolution of the laser measurements, the blades with tip pockets can easily be identified, because the rim surrounding the pocket causes the signal to peak twice whereas the pocket causes a trough between these two peaks. Taking the order of the blade and the direction of rotation into consideration, all blades can be identified.

5.3 Impact of Geometric Features

Figure 5.1 shows a typical laser probe response to the rotating turbine blades. As seen in Figure 5.1, the signal is equal to zero most of the time. The response to the passing blades is difficult to assess in this figure, because the signal is short. To make the response clearer and to be able to see the differences in the response to the different turbine blades, Figure 5.2 magnifies the peaks of each signal by magnifying the scale.

5.3.1 Effects of Surface Quality

The reflection of light strongly depends on the surface quality of the target. Although the tips of all turbine blades are polished to improve reflectiveness, there are still variations of reflectiveness on the surface of the blade tips. That is, the laser beam is reflected differently at different points on the surface of the blade tips and depending on this reflection, the amount of laser light detected by the laser probe varies. This explains the irregular pattern in the parts of the signal that correspond to the blade tips, e. g. the first and the last plot for the IBR 0.6 in in Figure 5.2. This effect also accounts for the difference in amplitude between the first and the last plot for the IBR 0.1 in in Figure 5.2.

5.3.2 Effects of Cross-Section & Tip Geometry

Since the laser beam is so tightly focused onto one spot-like point on the surface of the turbine disks, the signal exhibits higher resolution than the microwave signal. On the IBR 0.2 in, the IBR 0.2 in 30°, and the IBR 0.6 in, the signal clearly shows a response to the blade pockets – the signal rises as the laser beam is reflected on the

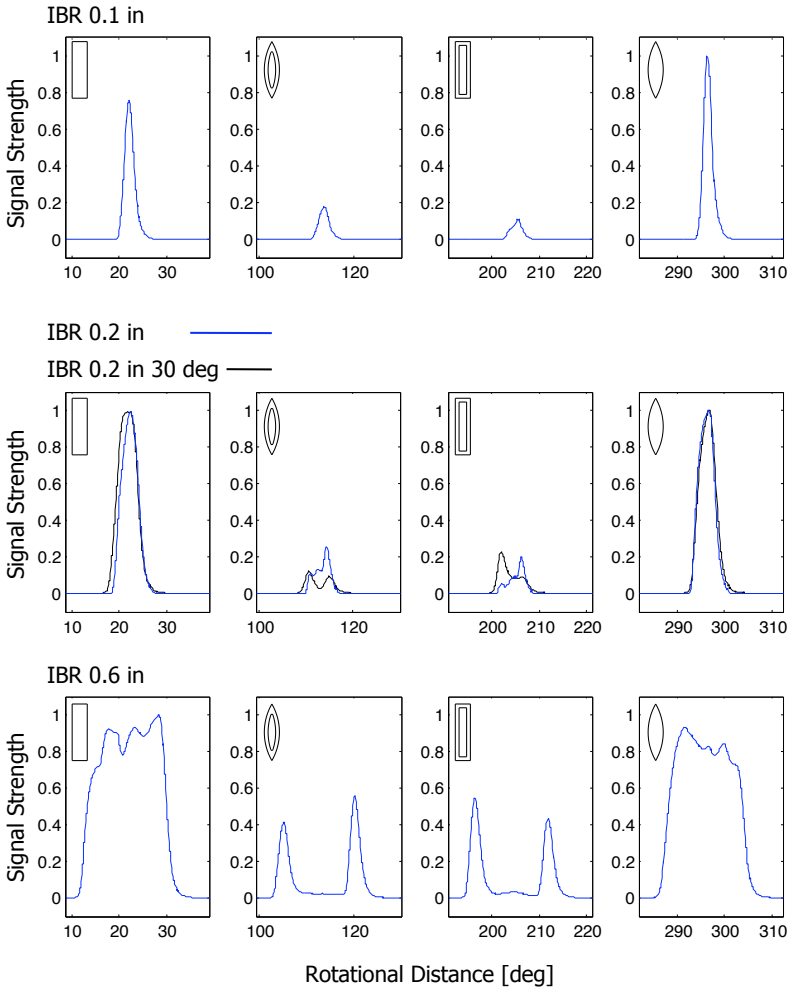

Figure 5.2: Magnification of the peaks in the laser signal. The schematics in the upper left corner of each plot represent the blade tip geometry

surface of the rims and falls as the laser beam is reflected on the surface within the pockets. It can also be seen that on the IBR 0.1 in, the pockets are not detected. The pockets on the 0.1 inch blades are too thin compared to the laser beam such that the pocket is spatially filtered out.

As a blade passes in front of the laser spot, the laser spot traces a line on the surface of the blade. This line is so thin that the trace of the laser is the same independent of variations of the cross-section, given that the width of the blade at the mid-blade is the same and the trace of the laser follows the mid-blade, see Figure 5.3.

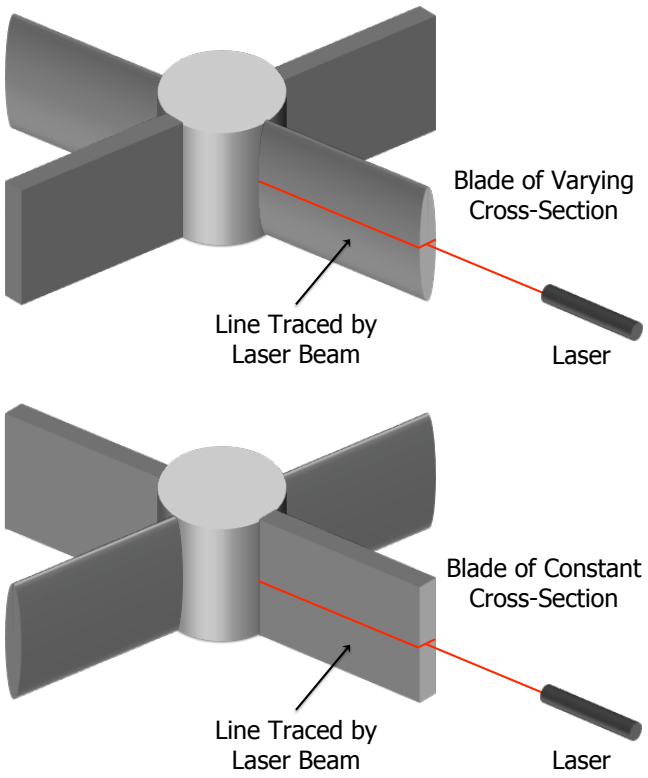

Figure 5.3: Effect of blade cross-section on laser measurements

5.3.3 Effects of Blade Width

The blade width only affects the measurement by affecting the length of time during which the spot is on the blade tips. As the blade passes, it causes a peak in the measured signal. A wider blade reaches the laser beam earlier and leaves it later than a thinner blade. Therefore, the signal has a peak for a longer time. As a result, the peaks caused by wider blades are wider than the peaks caused by thinner blades, compare Figure 5.2.

5.3.4 Effects of Chord Angle

As described in Section 4.4.3 and depicted in Figure 4.7, the chord angle of the blade affects the measurement by changing the length of time during which the blade is in front of the sensor. Consequently, the signal rises earlier and falls later. Therefore, the peaks caused by the blades with a chord angle are wider than the peaks caused by the blades without a chord angle, compare Figure 5.2. The angled blade is interpreted as a wider blade – from the measurement itself it cannot be deduced whether a chord angle or a larger width caused a wider peak.

5.4 Frequency Domain Analysis

Following the analysis of the signal in the time domain, this section presents the findings of the frequency domain analysis. Subsequently, the results are compared to the findings from the frequency domain analysis of the microwave signal.

The signals are windowed with a rectangular window that contains all four peaks. The sampling frequency at which the signal is acquired is 50 kHz. This number is caused by the rotational speed of 720 rpm and the fixed number of data points, 5000, acquired in 0.1 s. Figure 4.8 shows the resulting DFT for the IBR 0.1 in laser signal. The DFT of the IBR 0.1 in microwave signal is plotted for reference. Please see Appendix C for the DFTs of all IBRs.

The first significant peak occurs at a frequency of 48 Hz, which corresponds to the frequency at which the blades pass the sensor. The next weaker peaks occur at multiples of 48 Hz. From the analysis of Section 4.5.3, it appears that the peaks between these multiples are due to signal processing.

The DFT of the laser signal shows no evidence of excited eigenfrequencies. This conforms to the findings from the Campbell diagram analysis in Section 3.1.1, which show that no eigenfrequencies are excited at this low rotational speed.

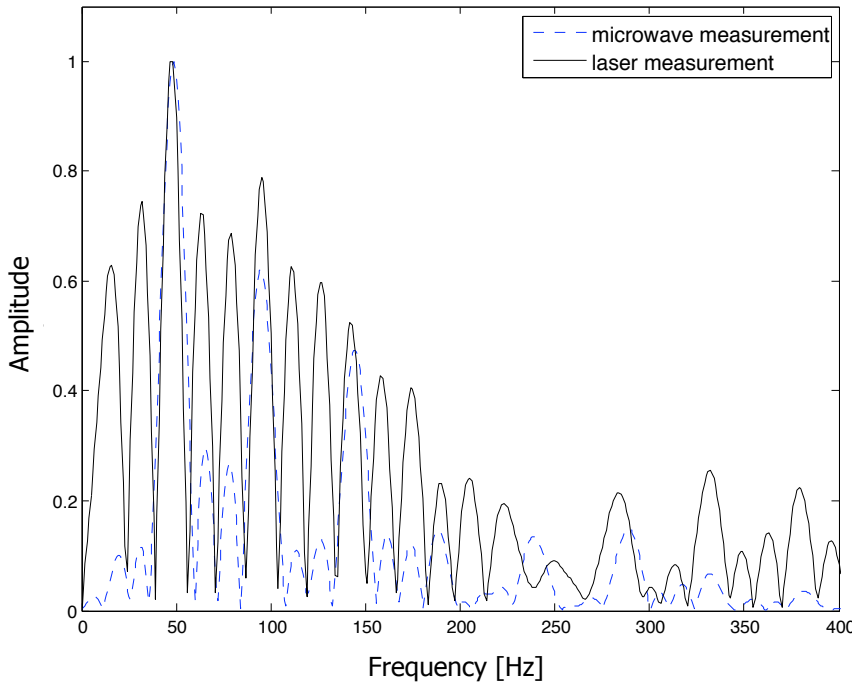

Figure 5.4: DFT of laser signal over one revolution measured on the IBR 0.6 in. The DFT of the IBR 0.6 in microwave signal is plotted for reference

All of these results correspond the results of the frequency domain analysis of the microwave signals from Section 4.5.1.

CHAPTER VI

CONCLUSION & FURTHER WORK

This chapter summarizes the research conducted and provides an outlook on future applications of the results obtained. The impact and contributions of the research are also presented.

6.1 Conclusion

This research investigates the the impact of turbine blade geometry on near-field microwave blade tip time of arrival measurements.

A literature review of existing ToA definitions is conducted. Considering accuracy, computational effort, and versatility of the definitions taken into consideration, the most viable approach in this definition is found to be the approach using constant fraction crossing as a trigger feature. Possible improvements to increase accuracy and versatility are suggested.

An experimental setup is designed and built that is capable of incorporating a range of different turbine disks, a microwave and an optical reference system and recording accurate signals that can be used for analysis.

A catalog of 16 turbine blade (tip-)geometries is developed. To gain a fundamental understanding of the microwave sensor response to a passing blade, the simplest geometries include blades with a rectangular cross-section of different widths. To

approach more realistic turbine blade geometries, varying cross-sections, blade tip pockets, and chord angles are added.

The signatures of the 16 passing turbine blades are acquired with both the optical and microwave probes and the impact of a change in the geometric features is investigated. Each passing blade causes a peak in the microwave time domain signal. The quality of the microwave results are found to be highly dependent on the angle between the direction of polarization of the microwaves and the turbine blade tip axis.

Analysis of the time domain signal shows that the widest blade with a rectangular cross-section causes the strongest sensor response. Decreasing the blade width, increasing the chord angle, or incorporating a blade tip pocket or a varying cross-section leads to a decrease in the amplitude of the peak caused by the blade. Increasing the blade width and incorporating a chord angle leads to an increase in peak width.

The low blade-width-to-sensor-aperture ratio results in a high degree of spatial filtering. Therefore, other than in the amplitude and width of the peaks, the geometric features are not reflected in the microwave signals with the exception of the widest blade with varying cross-section and blade tip pocket. The combination of these two features on the widest blade causes a change in the shape of the peak due to the higher blade-width-to-sensor-aperture ratio.

The frequency domain analysis is conducted on the microwave signals and verified with a synthetic signal. This analysis supports and confirms the findings from the time domain analysis.

The time domain analysis of the laser measurements shows that the spatial resolution of the laser is much higher than that of the microwave sensor. The rise and fall times of the signal are much shorter which is due to the much smaller field-of-view. Consequently, the signal acquired with the optical setup provides an accurate means

of defining the blade ToA satisfactorily and meets the requirements to fulfill the objective.

6.2 Outlook

This research is a stepping-stone towards the integration of field-ready microwave-based NSMS into turbine engines for the purpose of in-situ health monitoring.
As such, the conducted study expands the understanding of microwave sensors as part of non-optical blade ToA systems.

Possible next steps include the development of a predictive model of the airfoil-passing signature for rotating airfoils as they pass a stationary non-optical time of arrival probe. By simulating interaction of the microwaves with the turbine blade, such a model could predict blade passing signatures from an input of blade geometry and in this way, make use of the findings from this research.

In addition, the construction of the spin rig is designed to be very versatile. Although the blade geometries and the environmental conditions for the tests run in the scope of this research are relatively simple, the rig can also be used to investigate more complex rotors with a wide range of numbers of blades, blade geometries or blade materials at low cost compared to large-scale spin testing. In addition, the rig can be altered to allow for different environmental conditions by changing parameters like pressure or temperature. It even allows for the study of vibrations of turbine blades as part of PHM, e. g. in the scope of high cycle fatigue research.
Also, the spin rig is not limited to the types of sensors used in this research. It allows for investigations of a broad variety of contact and non-contact sensors and thus, opens up a wide range of possible research topics investigated using this spin rig.

6.3 Impact & Contributions

The research conducted expands the understanding of microwave sensors as part of non-optical blade ToA systems. Predicting the life of a gas turbine engine more accurately using such a non-optical system has three major impacts:

- **Higher durability:** Optical systems are of low durability, meaning they can only function correctly in a clean and calm environments whereas non-optical probes are not affected by dirt and the harsh environment in gas turbine engines. This allows for their eventual integration into a field-ready PHM system.

- **Increased safety:** This research will incorporate different blade geometries and broaden the knowledge about the acquired signals. Using this knowledge as a part of PHM can allow for a higher level of safety using gas turbine engines, because the onset of mechanical faults can be detected at a sufficiently early stage. This is achieved by integrating the already established knowledge about the relation between blade ToA, blade vibration, state of stress, and life prediction. Therefore, the level of safety can be improved in case failure occurs prior to the life predicted by conventional approaches as opposed to PHM

- **Reduced costs:** Conventional life predictions are made upon experience, extended time tests and approximation formulas. These life predictions are always very conservative and require the component or system to be replaced or maintained after a set amount of service hours. Often this maintenance or replacement is not necessary at this time due to the conservative life prediction. Keeping the component or system under permanent observation allows to extend the predicted life or maintenance intervals of servicing or replacing the component or system. Therefore, the costs can be reduced in case the gas

turbine engine does not require maintenance or a replacement after the life predicted by conventional approaches.

APPENDIX A

TECHNICAL DRAWINGS

The next few pages present the technical drawings of the four turbine disks used in this study.

Please note that the drawings are scaled to fit the layout of this thesis, such that the drawings are not to scale.

All dimensions are in inches.

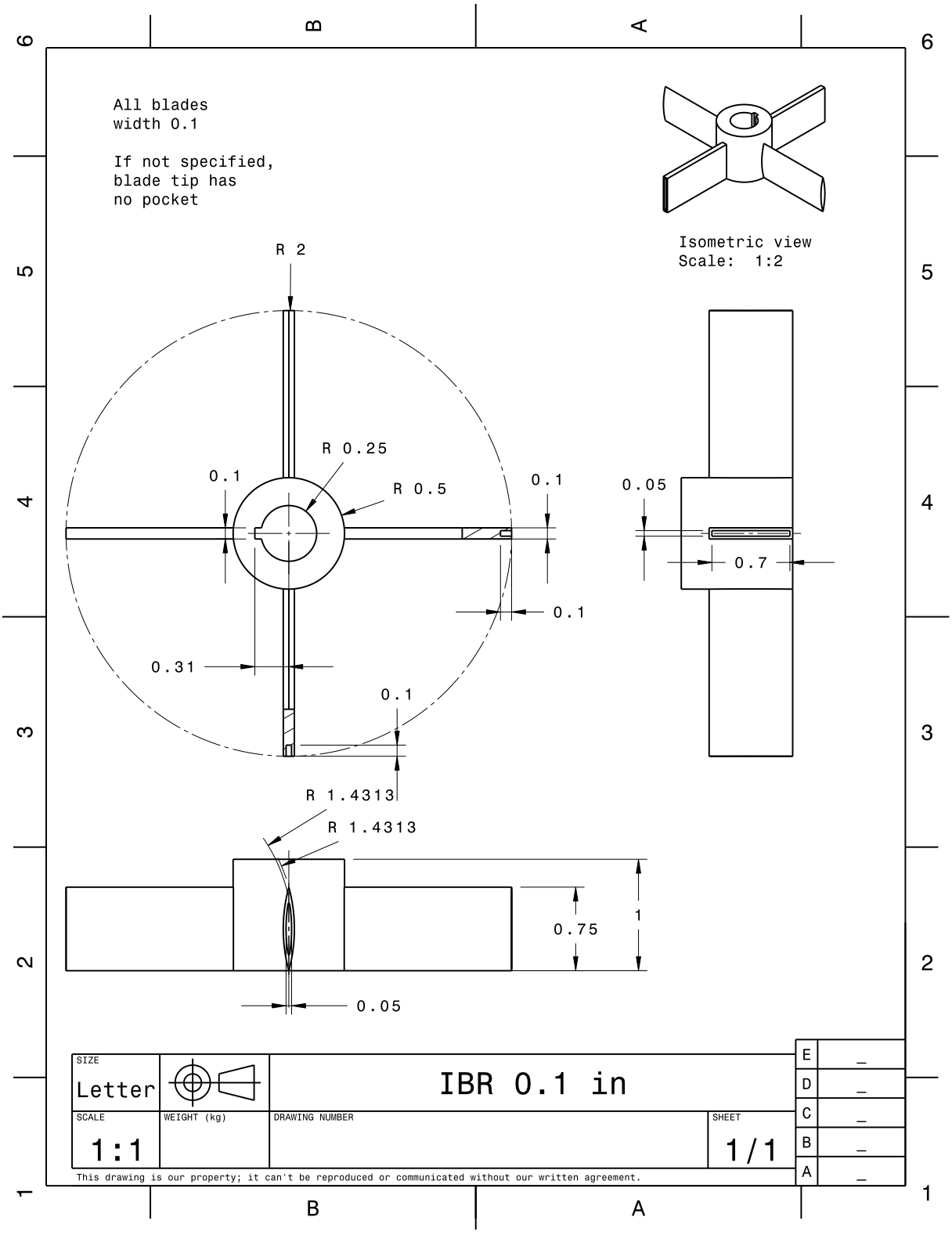

Figure A.1: Technical drawing of IBR with blade width 0.1 in

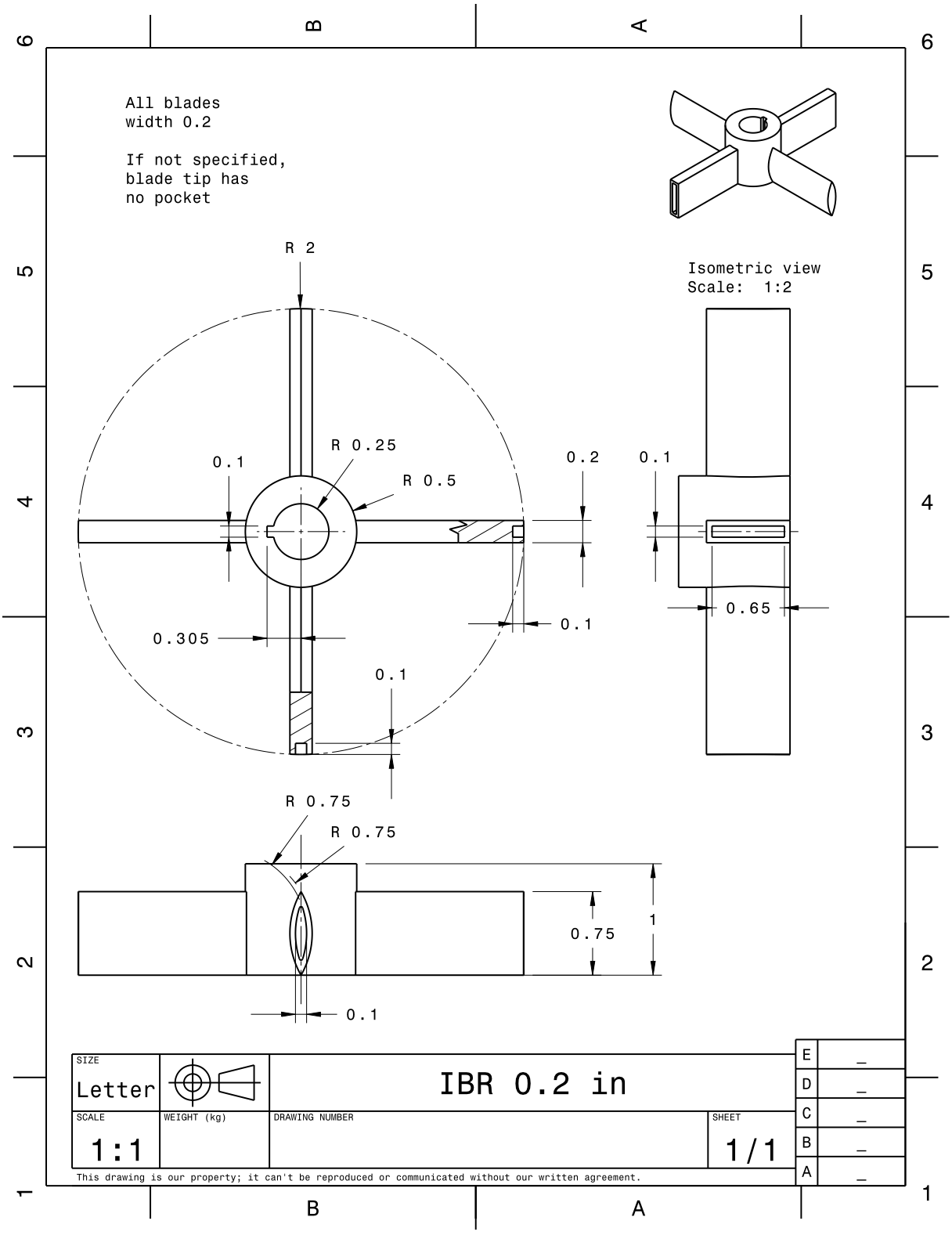

Figure A.2: Technical drawing of IBR with blade width 0.2 in

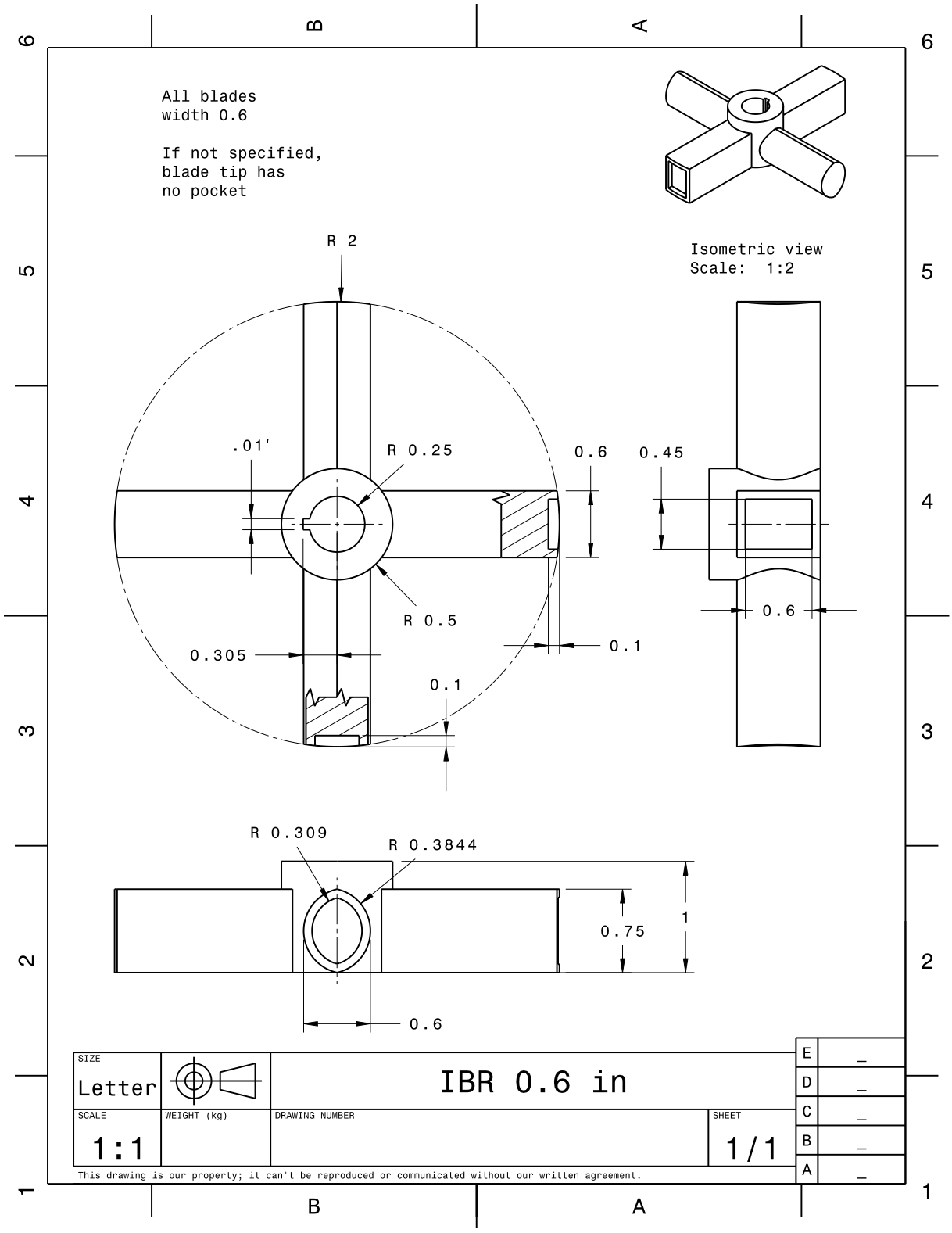

Figure A.3: Technical drawing of IBR with blade width 0.6 in

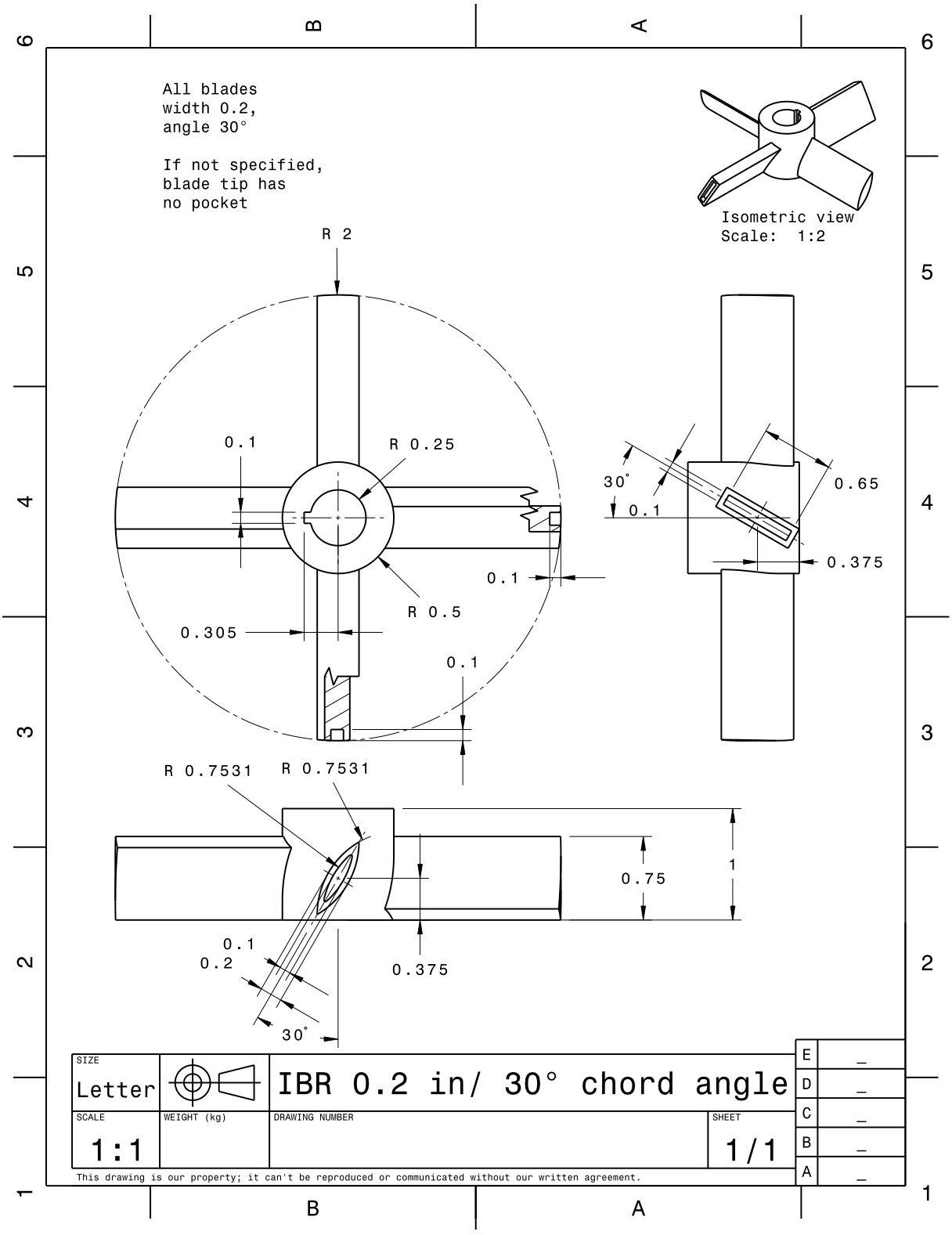

Figure A.4: Technical drawing of IBR with blade width 0.2 in and chord angle of 30°

APPENDIX B

TIME DOMAIN DATA

This appendix presents the microwave data used for blade identification.

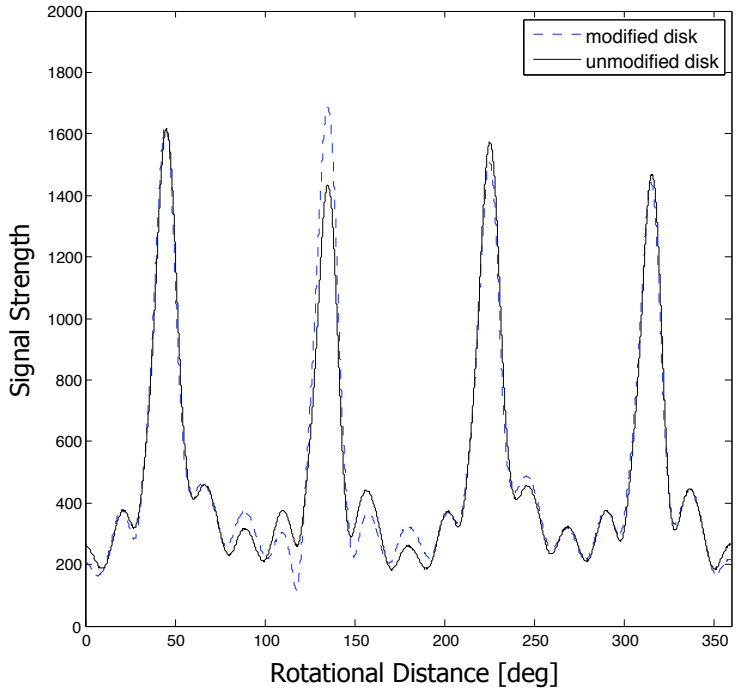

Figure B.1: Microwave measurements for blade identification on IBR with blade width 0.1 in

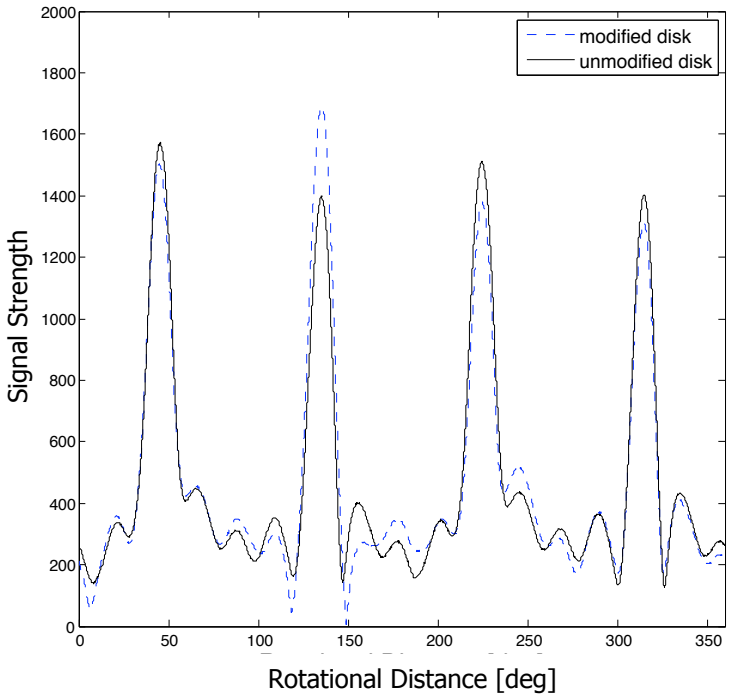

Figure B.2: Microwave measurements for blade identification on IBR with blade width 0.2 in

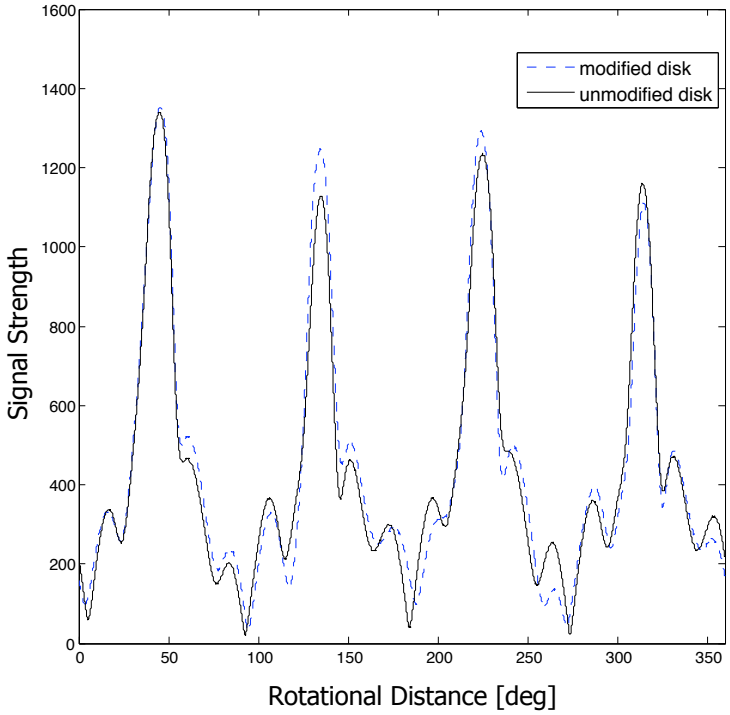

Figure B.3: Microwave measurements for blade identification on IBR with blade width 0.2 in and chord angle of 30°

APPENDIX C

FREQUENCY SPECTRA

This appendix presents the frequency domain analysis of both the microwave and the laser signals.

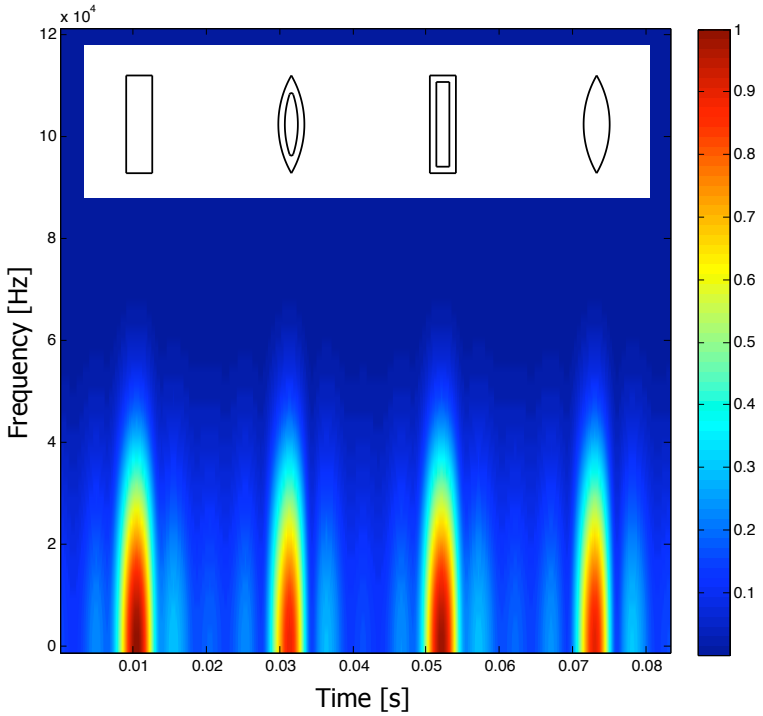

Figure C.1: STFT of microwave signal over one revolution (IBR with blade width 0.2 in)

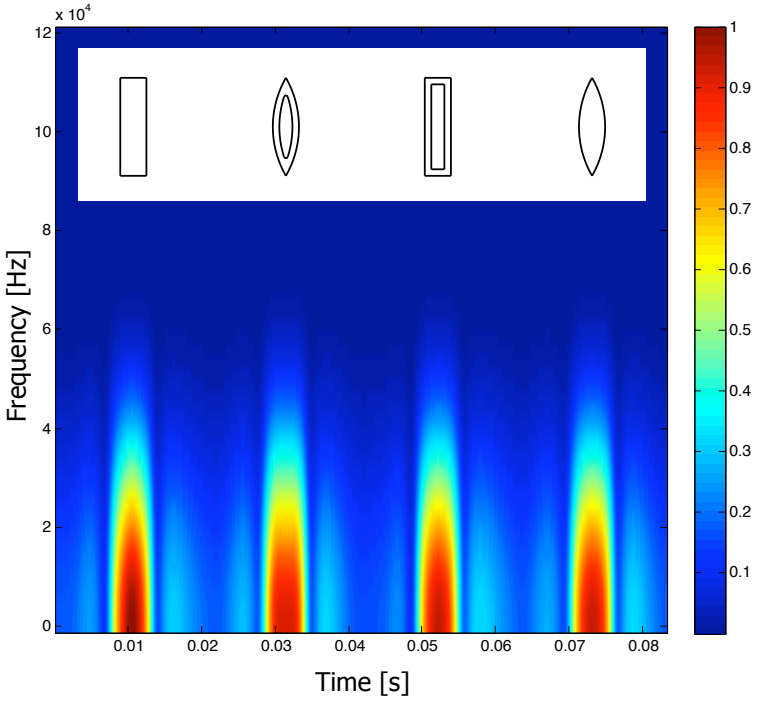

Figure C.2: STFT of microwave signal over one revolution (IBR with blade width 0.6 in)

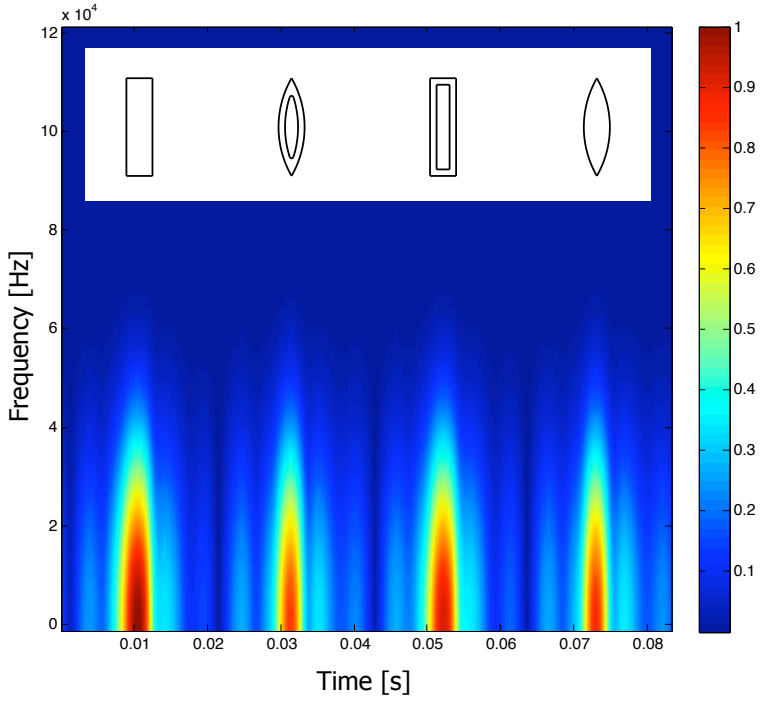

Figure C.3: STFT of microwave signal over one revolution (IBR with blade width 0.2 in) and chord angle of 30°

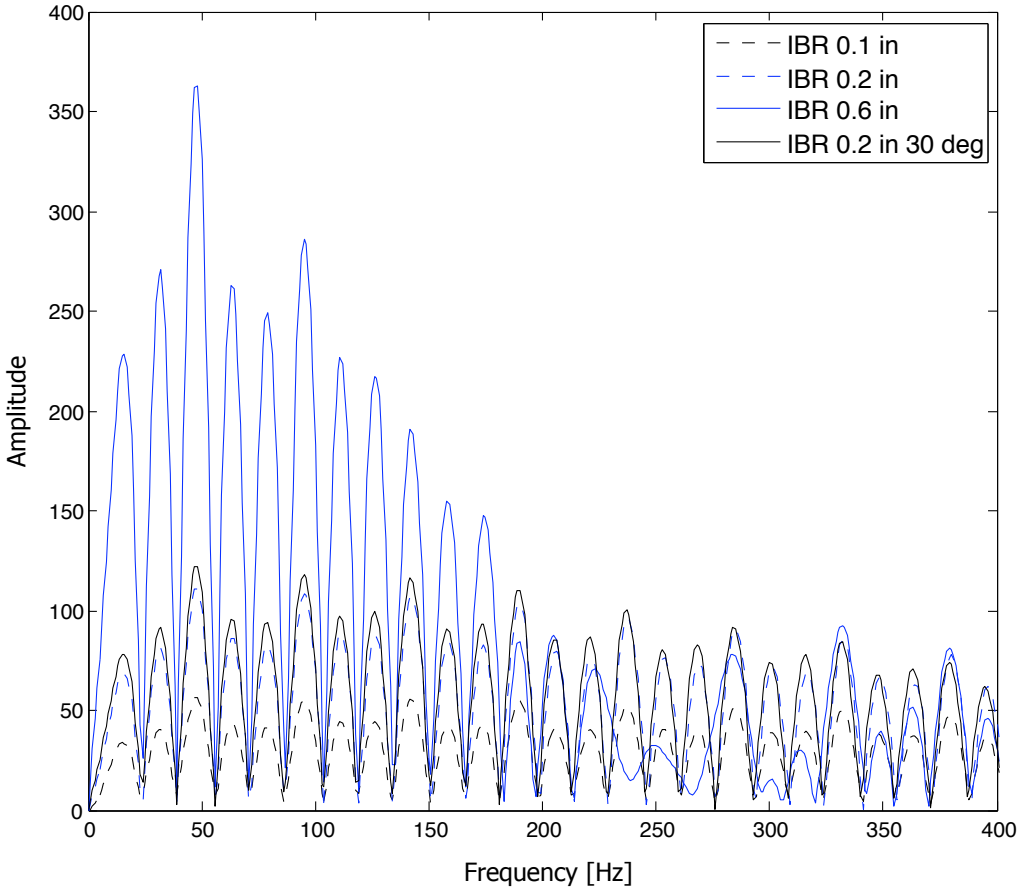

Figure C.4: DFT of laser signal over one revolution for each turbine blade

REFERENCES

[1] Agilis Measurememt Systems, "Non-intrusive stress measurement systems," *URL http://nsms.agilis.com*, June 2008.

[2] Christodoulou, L., "Prognosis," *Bidder's Conference and Workshop DARPA/DSO*, 2002.

[3] Cotgrove, R. M. and Wood, M. I., "Opportunities for advanced sensors for condition monitoring of gas turbines," *Opportunities and Advances in International Power Generation*, 1996.

[4] Den Hartog, J. P., *Mechanical Vibrations*. McGraw-Hill Book Company, Inc., 1956.

[5] Dimitriadis, G., Carrington, I. B., Wright, J. R., and Cooper, J. E., "Blade-tip timing measurement of synchronous vibrations of rotating bladed assemblies," *Mechanical Systems and Signal Processing*, 2002.

[6] Elmore, W. C. and Heald, M. A., *Physics of Waves*. Dover, 1969.

[7] Gallardo, J. M., Rodriguez, J. A., and Herrera, E. J., "Failure of gas turbine blades," *WEAR 252*, 2002.

[8] Giubbolini, L., "A multistatic microwave radar sensor for short range anticollision warning," *IEEE Transactions on Vehicular Technology*, 2000.

[9] Gould, R. G., "The laser, light amplification by stimulated emmision of radiation," *The Ann Arbor Conference on Optical Pumping, the University of Michigan*, 1959.

[10] Heath, S. and Imregun, M., "A survey of blade tip-timing measurement techniques for turbomachinery vibration," *Journal of Engineering for Gas Turbines and Power*, vol. 120, pp. 784 – 791, October 1998.

[11] Hess, A., "The prognostic requirement for advanced sensor and non-traditional detection technologies," *Prognosis Bidder's Conference DARPA/DSO*, 2002.

[12] Holmquist, E. B. and Jalbert, P. L., "Turbine blade tip clearance measurement instrumentation," *Proceedings of GT2007 ASME Turbo Expo 2007: Power for Land, Sea and Air*, 2007.

[13] Holst, T., "Analysis of spatial filtering in phase-based microwave measurements of turbine blade tips," Master's thesis, Georgia Institute of Technology, 2005.

[14] Jones, H., "Shedding light on vibration," *Mechanical Engineering*, 1996.

[15] Joung, K.-K., Paeng, K.-S., Choi, H.-J., Kang, S.-C., Park, N.-G., You, N.-J., and Von Flotow, A., "Analysis of vibration of the turbine blades using non-intrusive stress measurement system," *American Society of Mechanical Engineers, Power Division PWR, v2006, Proceedings of 2006 ASME Power Conference*, p. 7p, 2006.

[16] Laboratory for Atmospheric and Space Physics, "Electromagnetic spectrum," *URL http://lasp.colorado.edu/*, 2008.

[17] Littles, J. W., Pettit, R. G., Schirra, J. J., Cowles, B. A., Holmes, R. A., Russ, S. M., Rosenberger, A. H., and Larsen, J. M., "Demonstration of an advanced prognostic health management approach for gas turbine engines," *Materials Damage Prognosis*, 2005.

[18] Mazzucato, E., "Microwave imaging reflectometry for the visualization of turbulences in tokamaks," *Nuclear Fusion*, 2001.

[19] Oppenheim, A. V. and Schafer, R. W., *Discrete-Time Signal Processing*. Prentice Hall Signal Processing Series, 1998.

[20] Tappert, P., von Flotow, A., and Mercadal, M., "Autonomous phm with blade-tip sensors: Algorithms and seeded fault experience," *IEEE 0-7803-6599-2/01*, 2001.

[21] von Flotow, A., Tappert, P., Mercadal, M., Hardman, B., and Drumm, M., "Low cycle fatigue rotor burst prognosis using blade tip sensors," *Materials Damage Prognosis*, 2005.

[22] Wikipedia, "Laser," *URL http://en.wikipedia.org/wiki/Laser*, 2008.

[23] Zielinski, M. and Ziller, G., "Noncontact vibration measurements on compressor rotor blades," *Measurement Science and Technology*, vol. 11, pp. 847 – 856, July 2000.